ized anti–interleukin-6 receptor antibody: a multicenter, double-blind, placebo-controlled trial. Arthritis Rheum 2004;50:1761–9.
28. Schaller M, Burton DR, Ditzel HJ. Autoantibodies to GPI and creatine kinase in RA, and few human autoimmune sera detect GPI. Nat Immunol 2002;3:412–3.
29. Van Gaalen FA, Toes RE, Ditzel HJ, Schaller M, Breedveld FC, Verweij CL, et al. Association of autoantibodies to glucose-6-phosphate isomerase with extraarticular complications in rheumatoid arthritis. Arthritis Rheum 2004;50:395–9.
30. Kori Y, Matsumoto I, Zhang H, Yasukochi T, Hayashi T, Iwanami K, et al. Characterisation of Th1/Th2 type, glucose-6-phosphate isomerase reactive T cells in the generation of rheumatoid arthritis. Ann Rheum Dis 2006;65:968–9.
31. Maini R, St.Clair EW, Breedveld F, Furst D, Kalden J, Weisman M, et al, for the ATTRACT Study Group. Infliximab (chimeric anti-tumour necrosis factor α monoclonal antibody) versus placebo in rheumatoid arthritis patients receiving concomitant methotrexate: a randomized phase III trial. Lancet 1999;354:1932–9.
32. Lipsky PE, van der Heijde DM, St.Clair EW, Furst DE, Breedveld FC, Kalden JR, et al, for the Anti–Tumor Necrosis Factor Trial in Rheumatoid Arthritis with Concomitant Therapy Study Group. Infliximab and methotrexate in the treatment of rheumatoid arthritis. N Engl J Med 2000;343:1594–602.
33. Moreland LW, Baumgartner SW, Schiff MH, Tindall EA, Fleischmann RM, Weaver AL, et al. Treatment of rheumatoid arthritis with a recombinant human necrosis factor receptor (p75)-Fc fusion protein. N Engl J Med 1997;337:141–7.
34. Weinblatt ME, Kremer JM, Bankhurst AD, Bulpitt KJ, Fleischmann RM, Fox RI, et al. A trial of etanercept, a recombination tumor necrosis factor receptor:Fc fusion protein, in patients with rheumatoid arthritis receiving methotrexate. N Engl J Med 1999; 340:253–9.
35. Takagi N, Mihara M, Moriya Y, Nishimoto N, Yoshizaki K, Kishimoto T, et al. Blockage of interleukin-6 receptor ameliorates joint disease in murine collagen-induced arthritis. Arthritis Rheum 1998;41:2117–21.
36. Joosten LA, Helsen MM, van de Loo FA, van den Berg WB. Anticytokine treatment of established type II collagen–induced arthritis in DBA/1 mice: a comparative study using anti-TNFα, anti-IL-1α/β, and IL-1Ra. Arthritis Rheum 1996;39:797–809.

Mod Rheumatol (2008) 18:447–454
DOI 10.1007/s10165-008-0077-5

ORIGINAL ARTICLE

Retrospective clinical study on the notable efficacy and related factors of infliximab therapy in a rheumatoid arthritis management group in Japan: one-year outcome of joint destruction (RECONFIRM-2J)

Tsutomu Takeuchi · Hisashi Yamanaka · Eisuke Inoue · Hayato Nagasawa · Masao Nawata · Katsunori Ikari · Kazuyoshi Saito · Naoya Sekiguchi · Eri Sato · Hideto Kameda · Shigeru Iwata · Takeshi Mochizuki · Kouichi Amano · Yoshiya Tanaka

Received: 11 March 2008 / Accepted: 21 March 2008 / Published online: 21 May 2008
© Japan College of Rheumatology 2008

Abstract The anti-TNF-α chimeric monoclonal antibody infliximab is the first biologic to be approved for rheumatoid arthritis (RA) in Japan, and post-marketing surveillance of all of the Japanese cases treated with infliximab has been conducted to explore the safety of infliximab therapy. In addition, a retrospective clinical study on the notable efficacy and related factors of infliximab therapy in an RA management group in Japan (RECONFIRM and RECONFIRM-2) has demonstrated clinical responses. However, information on the effect of infliximab on joint destruction in Japanese RA patients remains insufficient. In this study, we retrospectively analyzed X-ray data from 67 patients in whom both hand and foot X-rays at baseline and at 54 weeks had been available among the 410 cases in the RECONFIRM-2 study. By scoring the X-rays according to the modified van der Heijde (vdH)–Sharp method, we found that the total vdH–Sharp score in the RA patients before infliximab therapy was 104.40 ± 87.34 and the yearly progression was 21.33, indicating relatively rapid progression. After infliximab therapy for 54 weeks, the total vdH–Sharp score at 54 weeks was 104.37 ± 86.87 and the estimated yearly progression was −0.03, indicating the almost complete inhibition of progression. The RECONFIRM-2J study confirmed the significant ability of infliximab to halt joint destruction in Japanese RA patients, and showed that joint destruction was significantly associated with disease activity and the dose of MTX in the patients with moderate and advanced disease durations, respectively, before infliximab therapy.

Keywords Rheumatoid arthritis · Infliximab · Total van der Heijde–Sharp score · Joint destruction

T. Takeuchi (✉) · H. Nagasawa · N. Sekiguchi · H. Kameda
Department of Rheumatology and Clinical Immunology, Saitama Medical Center, Saitama Medical University, 1981 Tsujido-machi, Kamoda, Kawagoe, Saitama 350-8550, Japan
e-mail: tsutake@saitama-med.ac.jp

M. Nawata · K. Saito · S. Iwata · K. Amano · Y. Tanaka
The First Department of Internal Medicine, School of Medicine, University of Occupational and Environmental Health, Kitakyushu, Japan

H. Yamanaka · E. Inoue · K. Ikari · E. Sato · T. Mochizuki
Institute of Rheumatology, Tokyo Women's Medical University, Tokyo, Japan

Introduction

Rheumatoid arthritis (RA) is a systemic inflammatory disorder, characterized by chronic, destructive and deforming arthritis [1], resulting in significant morbidity and mortality [2–5]. Since TNF-α plays a pivotal role in the pathogenesis of RA [6–8], biological agents targeting TNF-α are highly effective at not only reducing clinical signs and symptoms but also retarding structural damage to the joints; thus, these agents have had a great impact on the management of RA [9]. The abovementioned results were obtained in double-blind, randomized, clinical trials in which methotrexate (MTX; mean weekly doses ranging between 15 and 17 mg) and infliximab were administered concomitantly [10–12]. In Japan, however, the maximal approved dose of MTX is 8 mg/week; this difference raises the question of whether infliximab can suppress joint destruction when a lower dose of MTX is being administered concomitantly, as is the case in daily clinical practice in Japan.

The anti-TNF-α chimeric monoclonal antibody infliximab is the first biologic to be approved for the treatment of

RA in Japan [13], and the approved dose is 3 mg/kg every eight weeks after zero, two, and six weeks of induction with MTX. The safety of infliximab use in Japan has now been explored in a post-marketing surveillance of all of the cases that have been treated with infliximab [14]. Furthermore, a retrospective clinical study on the notable efficacy and related factors of infliximab therapy in a RA management group in Japan (RECONFIRM) has demonstrated clinical responses, with significant improvements observed in 258 cases after 22 weeks [15] and extended observations from 22 to 54 weeks completed in 410 cases (RECONFIRM-2) [16]. The RECONFIRM-2 study has shown that the retention rate at 54 weeks was 75.6% and that European League Against Arthritis (EULAR) good, moderate and no responses to infliximab were 37.0, 41.7 and 21.2%, respectively, with EULAR remission achieved in 27.6% of patients; thus, these data confirmed the excellent clinical efficacy of infliximab when administered over a period of one year [16]. However, information on the effect of infliximab on joint destruction in Japanese RA patients remains insufficient.

In a previous study, we demonstrated that the estimated yearly progression rate was extremely high in Japanese RA patients before the start of infliximab therapy [17], and that the progression rate was suppressed by treatment with infliximab for one year [17]. This data was collected at a single center, and the patients who were recruited for the study were longstanding RA patients who had been waiting for a long time for anti-TNF inhibitors to be approved. Consequently, any interpretation of these results is limited. In the present RECONFIRM-2J study, we recruited 67 of the 410 cases reported in the RECONFIRM-2 study [16]; these patients were recruited from three centers, and 19.4% had early RA ($\leq$2 years). Both hand and foot X-rays at baseline and at 54 weeks were available for all of the recruited patients. We then retrospectively analyzed the X-ray data from these 67 patients before and 54 weeks after the start of infliximab therapy using a modified van der Heijde (vdH)–Sharp score. The factors contributing to the progressive features of joint destruction at baseline as well as those at 54 weeks after infliximab therapy were then analyzed.

Patients and methods

Patients and evaluation

Data and information on RA patients fulfilling the diagnostic criteria of the American College of Rheumatology (ACR) [18] were collected from three major rheumatology centers in Japan: the Department of Rheumatology and Clinical Immunology, Saitama Medical Center, Saitama Medical University, Saitama; the First Department of Internal Medicine, School of Medicine, University of Occupational and Environmental Health Japan, Kitakyushu; and the Institute of Rheumatology, Tokyo Women's Medical University. All patients receiving infliximab treatment at one of these institutions as of December 2005 were registered in this retrospective study. Demographic data, including disease duration and concomitant therapy, were collected from the patients' medical charts. The following parameters were evaluated before and at 54 weeks after the initial infliximab infusion: tender joint count (TJC) 28, swollen joint count (SJC) 28, patient's assessment of pain on a visual analog scale (patient's pain VAS), patient's global assessment of disease activity (patient's global VAS), physician's global assessment of disease activity (physician's global VAS), and C-reactive protein (CRP).

Infliximab therapy

Infliximab was infused to patients at zero, two, and six weeks followed by every eight weeks at a dose of 3 mg/kg, according to the drug labeling and the guidelines of the Infliximab Study Group of the Ministry of Health, Welfare and Labor in Japan [19]. The concomitant use of MTX was instituted in all cases, although the dose of MTX was determined by each attending physician.

Therapeutic response

Disease activity was assessed using the disease activity score, including a 28-joint count (DAS28)-CRP that was calculated according to the authorized formula (http://www.das-score.nl/www.das-score.nl/index.html). DAS28-CRP values are reportedly lower than the original DAS28 assessments using the erythrocyte sedimentation rate (ESR), and we used a threshold of 4.1, instead of the original 5.1, as the cut-off for high activity and 2.7, instead of 3.2, as the cut-off for low activity [20]. Thus, we defined DAS28-CRP values $\geq$4.1 as high activity, $\leq$2.7 to $<$4.1 as moderate activity, and $<$2.7 as low activity, with $\leq$2.3 defined as remission [15, 16]. The responses to infliximab therapy at 22 weeks were evaluated using the European League Against Arthritis (EULAR) response criteria, with 4.1 and 2.7 used as the thresholds for high and low disease activities, respectively.

X-ray evaluations of hand and feet joints

Among the 410 patients in the RECONFIRM-2 study, X-ray images of both hands and feet at 0 and 54 weeks were available for 67 patients. Two expert readers independently scored articular damage and progression in a

blinded fashion according to the modified vdH–Sharp scoring method. Radiographic progression was defined as a difference that was greater than the smallest detectable difference (SDD) [21]. The SDD for the mean change from baseline using the two readers' scores for each patient's radiographs was 4.39 (the standard deviation of the per-patient differences between the readers divided by the square root of 2), which corresponds to nearly 1% of the maximum total modified vdH–Sharp score (TSS)—that is, 448.

Statistical analysis

Patients with radiographs of both hands and feet at baseline and at 54 weeks after the start of infliximab therapy were included in the analysis. Summary statistics of the median, mean, and interquartile ranges are presented for continuous variables. Spearman correlation analyses were performed to evaluate the association between baseline covariates and changes in the radiographic scores. For categorical response parameters, group comparisons were made using the chi-square test. Logistic regression analyses were performed to examine the significance of individual variables in predicting radiographic progression at baseline and at week 54. Patients were grouped into tertiles according to key predictors identified by the correlation and regression analyses at baseline; changes in total modified vdH–Sharp score (TSS) were summarized for the patients in each tertile.

The proportions of patients who had no progression in their TSS and joint space narrowing score were calculated. No progression was defined as less than 0.5 units of change from baseline or less than a given threshold value, such as the SDD, in their TSS.

Statistical analyses were performed using JMP software version 6.1 (SAS Institute, Cary, NC, USA). All statistical testing was two-sided. P values ≤ 0.05 were considered significant.

Results

Baseline demographics and subsequent changes in clinical parameters for 67 patients with X-ray data

Among the 410 patients enrolled in the RECONFIRM-2 study, we selected 67 patients in whom both hand and foot X-ray data were available and investigated structural damage and its progression during infliximab therapy in this RECONFIRM-2 Joint (RECONFIRM-2J) study. When the baseline characteristics of the 67 patients in the RECOMFIRM-2J study were compared with the rest of the patients in the RECONFIRM-2 study without X-ray data ($n = 343$), the patients in the present study were found to be younger and received higher doses of MTX than the 343 patients without X-ray data in the RECONFIRM-2 study (Table 1). Age and dose of MTX were significantly different between the patients in the RECONFIRM-2J study and the rest of the patients in the RECONFIRM-2 study (age: 50.8 ± 11.4 vs. 53.7 ± 12.9 years, respectively, $P = 0.0411$; MTX dose: 8.3 ± 2.4 vs. 7.7 ± 1.9 mg, respectively, $P = 0.0349$). As shown in Table 1, the clinical parameters of the 67 patients in the present study responded dramatically to infliximab therapy (DAS28 at 0 week: 5.64 ± 1.03, and DAS28 at 54 weeks: 3.02 ± 1.25; 46.5% reduction), and the response rate was slightly better than that of the 343 patients in the RECONFIRM-2 study (DAS28 at 0 week: 5.48 ± 1.14, and DAS28 at 54 weeks: 3.34 ± 1.41; 39.1% reduction).

Baseline X-ray data

Joint destruction was assessed using the modified vdH–Sharp score of hand and foot X-rays at baseline (0 week) and at 54 weeks after the start of infliximab therapy. The score at 0 week ranged from 9.5 to 410. The mean $\pm$ SD of the score at baseline was 104.40 ± 87.34, and the median, upper quartile, and lower quartile values were 73.5, 147.5, and 45.0, respectively. When the estimated yearly progression from disease onset was calculated, its value ranged from 2.11 to 118.80, with a mean value of 21.33. The median, upper quartile, and lower quartile values of the estimated yearly progression in the patient cohort were 16.19, 25.50, and 9.69, respectively.

To clarify the clinical parameters related to the total modified vdH–Sharp score (TSS) before infliximab therapy, we analyzed a possible correlation between the TSS and a series of clinical parameters at 0 weeks. No significant relations between the TSS at 0 weeks and sex, age, RF titer, DAS28, MTX dose, or PSL dose at 0 weeks were found, whereas the TSS at 0 weeks was significantly correlated with the disease duration ($r = 0.62$, $P < 0.001$). Since these factors interact with each other, we analyzed the relationship between the TSS and a series of clinical parameters at 0 weeks using a multivariate analysis but found no significant correlation among the parameters, with the exception of disease duration again (data not shown). Thus, we further analyzed the possible correlation between TSS and a series of clinical parameters at 0 weeks in subgroups of the patients with variable disease durations.

Correlation between total modified vdH–Sharp score and clinical characteristics among patients with variable disease durations before infliximab therapy

Since disease duration was the only factor significantly correlated with the total modified vdH–Sharp score (TSS)

Table 1 Clinical characteristics in RECONFIRM-2J and RECONFIRM-II studies

Variables	RECONFIRM-2J ($N = 67$)					The other cases in RECONFIRM-2 ($N = 343$)					P value
	Mean	SD	Median	25%	75%	Mean	SD	Median	25%	75%	
Female	0.91	–	–	–	–	0.86	–	–	–	–	0.4216
RF(±)	0.84	–	–	–	–	0.88	–	–	–	–	0.3095
Age	50.8	11.4	53	44.5	59.5	53.7	12.9	56	46	63	0.0411
Duration	7.9	7.3	5.6	2.5	10.8	9.8	9.1	7.0	3.0	14.0	0.1549
Stage	3	1	3	2	4	3	1	3	2	4	0.4893
Class	2	1	2	2	3	2	1	2	2	2	0.0553
RF	169.5	230.9	68.5	32.0	207.2	222.2	352.0	99.3	40.6	243.9	0.2484
MTX dose	8.3	2.4	8	8	8	7.7	1.9	8	6	8	0.0349
PSL dose	4.4	3.2	5.0	1.5	6.5	3.7	3.8	4.0	0.0	5.0	0.0574
CRP	3.8	3.1	2.8	1.5	5.3	3.2	2.7	2.5	1.0	4.6	0.1969
TJC	11.1	6.9	10	6	17	10.3	7.3	9	5	14	0.2607
SJC	10.9	5.6	10	7	15	10.5	6.3	9	6	14	0.3115
GH	61.0	22.4	63	47	79	63.7	21.5	67	50	80	0.3081
DAS0	5.6	1.0	5.7	4.9	6.5	5.5	1.1	5.5	4.7	6.3	0.2967
DAS2	3.5	1.1	3.6	2.8	4.3	3.4	1.2	3.3	2.6	4.2	0.3587
DAS6	3.2	1.1	3.1	2.6	3.9	3.2	1.2	3.2	2.3	4.0	0.9418
DAS14	3.1	1.2	3.0	2.2	3.7	3.3	1.4	3.1	2.3	4.1	0.2938
DAS22	3.0	1.2	2.8	2.0	3.9	3.4	1.5	3.3	2.2	4.4	0.1108
DAS30	3.0	1.2	3.1	2.2	3.7	3.4	1.4	3.4	2.3	4.4	0.0576
DAS38	3.1	1.2	3.1	2.4	3.9	3.4	1.4	3.2	2.3	4.2	0.2846
DAS46	3.2	1.2	2.9	2.3	4.0	3.3	1.4	3.1	2.2	4.2	0.7174
DAS54	3.0	1.2	2.7	2.2	3.7	3.3	1.4	3.3	2.2	4.3	0.0795

at 0 weeks, we attempted to categorize the patients into three groups by the disease duration according to the lower quartile (2.5 years) and the upper quartile (11.0 years) of the distribution (Fig. 1a). The three groups of the patients, thus, subdivided into early (≤2.5 years), moderate (>2.5 to ≤11.0 years), and advanced disease (>11.0 years) clearly showed that the estimated yearly progression was most rapid in the early RA (Fig. 1b). In the early RA group (disease duration ≤2.5 years), no significant correlations between the TSS at 0 week and a series of clinical parameters were found, whereas the DAS28 at 0 weeks was significantly correlated with the TSS at 0 weeks in the moderate RA group ($r = 0.416$, $P = 0.015$); the dose of MTX was also inversely correlated with TSS at 0 weeks in the advanced RA group ($r = -0.508$, $P = 0.045$) (Fig. 2).

X-ray progression at 54 weeks after the start of infliximab therapy

After treatment with infliximab, the total modified vdH–Sharp score (TSS) at 54 weeks was not markedly progressed and remained unchanged from that at 0 weeks (104.40 ± 87.34 at 0 weeks vs. 104.37 ± 86.87 at 54 weeks), as shown in Fig. 3. The estimated yearly progression at 0 weeks was 21.33, while that at 54 weeks was −0.03, producing a 101.14% reduction in the rate of joint destruction. In addition, progression was completely inhibited in 39 patients (58.2%), including 25 patients (37.3%) with negative changes—suggesting the possibility of radiographic repair. No new erosions were seen in 66 patients (98.5%), and only one patient, in whom estimated yearly progression at 54 weeks was 7.5, exhibited new erosions. These results confirm that infliximab therapy strongly inhibited the progression of structural damage, even in Japanese RA patients with high estimated yearly progression rates of over 20 and mean disease durations of around ten years (13 cases, 19.4% of the total of 67 cases, were early RA with disease duration ≤2 years).

Finally, we investigated the possible correlation between the estimated yearly progression at 54 weeks and a series of clinical parameters and found that sex, age, disease duration, RF titer, MTX dose, and PSL dose were not significantly correlated with the progression of joint destruction (data not shown), suggesting that infliximab therapy suppressed the progression of structural damage remarkably in the vast majority of the patients, irrespective of the clinical characteristics of the patients. In addition, the estimated yearly progressions at baseline for the

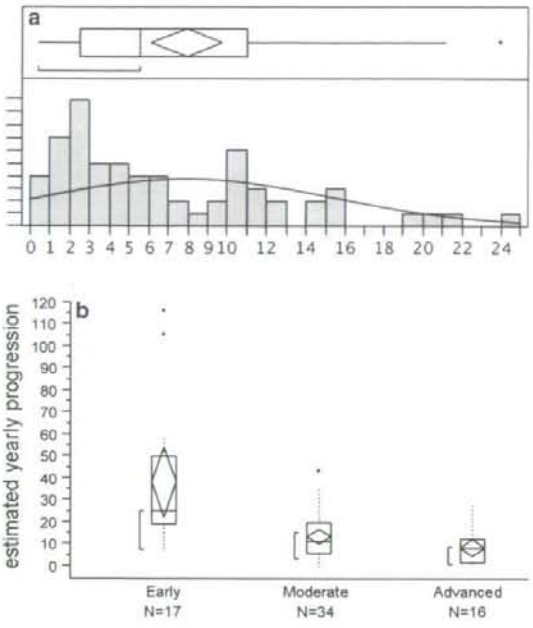

Fig. 1 **a** Number of cases with early, moderate or advanced RA. The *line* in the *box* represents the median value, the *diamond box* represents the mean value, and the upper and lower ends of the *box* indicate the 25th and 75th percentiles of the population. **b** Yearly progression of TSS in patients with early RA ($n = 17$), moderate RA ($n = 34$), and advanced RA ($n = 16$). The *line* in the *box* represents the median value, and the upper and lower ends of the *box* indicate the 25th and 75th percentiles of the population

patients with early, moderate, or advanced RA were significantly suppressed at 54 weeks, as shown in Fig. 3 (0.21 ± 0.60, -0.11 ± 0.42, and -0.09 ± 0.62, respectively), indicating that infiximab effectively halted the progression of structural damage not only among patients with advanced diseases but also among patients with early or moderate disease.

Discussion

The RECONFIRM-2J study analyzed structural damage in Japanese RA patients who had been treated with infliximab in addition to low doses of MTX and examined the clinical parameters correlated with joint destruction. Although the clinical efficacy and safety of infliximab therapy in Japanese patients with RA has now been explored [15, 16], only a few reports have examined the effect of infliximab on structural damage [17]. In this report, we studied 67 RA patients among the 410 patients enrolled in the RECONFIRM-2 study and analyzed the structural damage in these patients using the modified vdH–Sharp scoring method at 0 weeks as well as at 54 weeks after the start of infliximab therapy. The average total modified vdH–Sharp score (TSS) at baseline was 104.40 and the estimated yearly progression was 21.33 prior to the start of infliximab therapy, whereas the average TSS was markedly suppressed to 104.37 and the estimated yearly progression was −0.03 at 54 weeks after the start of infliximab therapy.

This study has several limitations. First, among the 410 enrolled RA patients in the RECONFIRM-2 study, we retrospectively analyzed 67 patients for whom hand and foot X-rays taken at 0 and 54 weeks after the start of infliximab therapy were available. So, a possible selection bias should be seriously considered. Although the patients in this study were younger and the doses of MTX were greater than those without X-ray analysis, the other baseline characteristics and clinical parameters were comparable among two groups. On the other hand, the response to infliximab was slightly better among the 67-patient cohort in the present study, introducing the possibility that we may have selected patients with a better response to therapy. Nevertheless, when the responses were assessed using the ACR and EULAR criteria, the differences in the responses of the two patient populations were not significantly different. Second, the dose of MTX used in Japan is lower than those used in other countries, including the US, many European countries and even other Asian countries, because of a Japanese regulatory restriction stating that the maximum allowable dose of MTX is 8 mg/week; nevertheless, higher doses of MTX are sometimes used in daily clinical practice. Indeed, the mean MTX dose in the present study was 8.3 mg/week, which was still almost half of that used in double-blind, randomized clinical trials for infliximab [10–12, 22]. However, these circumstances provide an interesting opportunity to examine X-ray progression during infliximab therapy administered concomitantly with low-dose MTX. In addition, the present study appears to reflect daily clinical practice, whereas most studies showing the efficacy of anti-TNF biologics on joint destruction have been derived from randomized controlled trials [10–12, 22].

The X-ray progression of the Japanese RA patients was considerably rapid. Although the mean duration of the disease in these patients was 7.9 years, the estimated yearly progression, which was calculated using the total modified vdH–Sharp score at baseline divided by the disease duration, was 21.33. Since we were utilizing a 448 full-scale scoring system, 21.33 correspond to 4.76% of the full scale. The estimated yearly progression in the ATTRACT study was 7.06, corresponding to 1.61% of a 440 full-scale scoring system. These results suggest that structural damage progressed three times more rapidly in the present study than in previous American and European studies. To interpret the above results carefully, we compared the clinical characteristics of the RECONFIRM-2J and

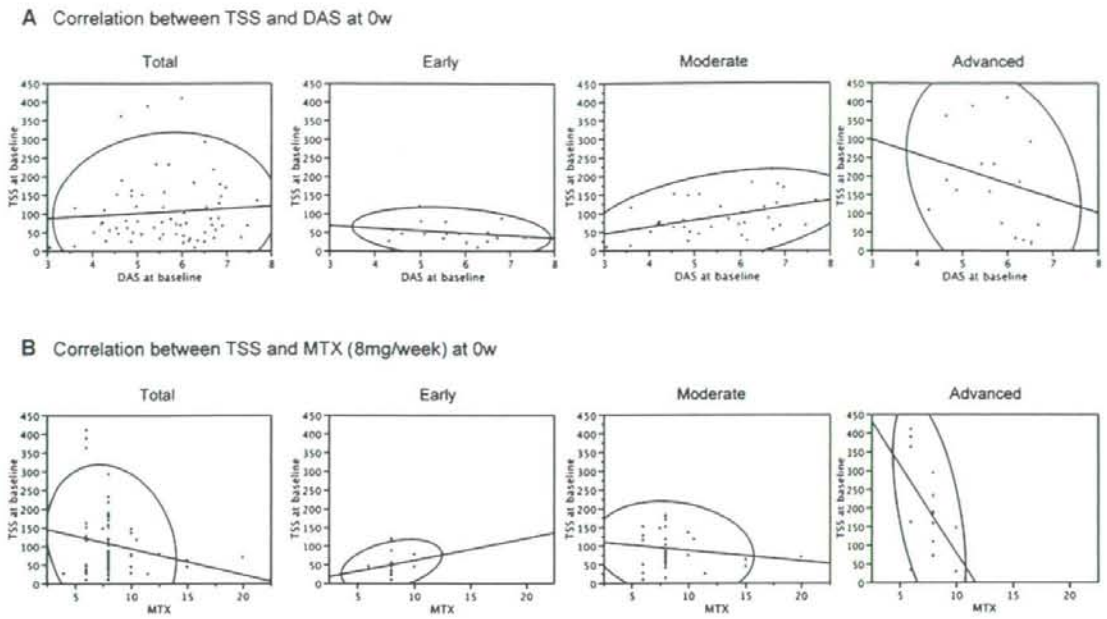

Fig. 2 **a** Correlation between DAS28 at 0 weeks and TSS at 0 weeks in a group of patients with RA. **b** Correlation between MTX dose (mg/week) and TSS at 0 weeks in a group of patients with RA. The *circle* represents the 95% confidence area

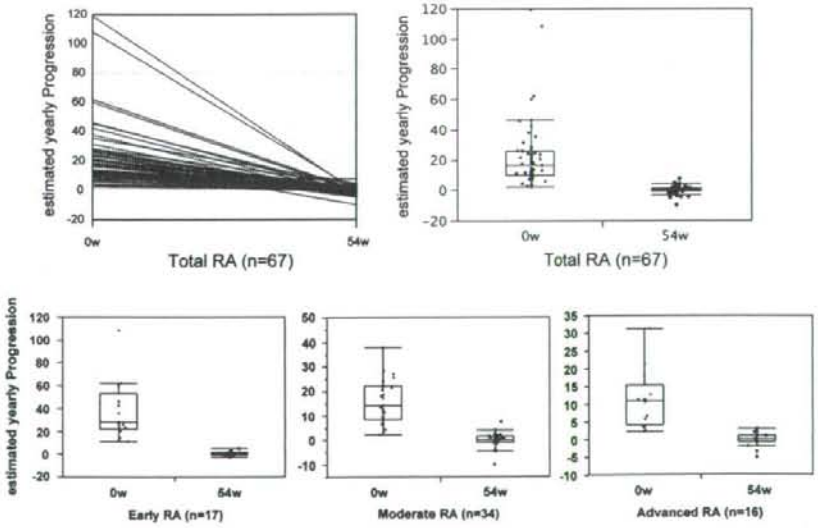

Fig. 3 *Left* Yearly progression of TSS in an individual patient at 0 and 54 weeks after the start of infliximab therapy. The *line* in the *box* represents the median value, and the upper and lower ends of the *box* indicate the 25th and 75th percentiles of the population

ATTRACT studies (Table 2) and found several differences in patient background characteristics, such as female dominance (91 vs. 78%), a shorter disease duration (7.94 vs. 10.84 years), earlier stage RA (% of patients with a disease duration of less than 3 years: 34.3 vs. 13.4%), and a lower dose of MTX (8.27 vs. 16.19 mg/week). Since joint destruction progresses rapidly during the initial 1–2 years after onset when patients are treated using conventional DMARD therapy [23, 24], these data imply that the patients enrolled in the RECONFIRM-2J study, who had a relatively short disease duration, likely exhibited a more rapid disease progression than those in the ATTRACT study. Nevertheless, we should seriously consider the possibility that Japanese RA patients may exhibit

Table 2 Clinical and radiographical characteristics in RECONFIRM-2J and ATTRACT

	Clinical and radiographical characteristics	
	RECONFIRM -2J	ATTRACT, 3 mg/kg/8 weeks group
Age	51	54
Female (%)	91	81
Duration (year)	8	10
Early RA patients (<3y, %)	34.3	13.4
Patients with RF (%)	84	84
Average dose of MTX (mg/week)	8	16
Patients with PSL (%)	76	63
Mean TSS at baseline/full score	104/448	79/440
Full scale (%)	23.21	17.95
Mean estimated yearly progression/full scale	21.3/448	7.9/440
Full scale (%)	4.76	1.80
Patients with improve (%)	37	44
Patients with a aggravation (%)	1.5	8.0
Change in TSS during 54 week	−0.03	1.3

rapid X-ray progression. In the Japanese SAMURAI study, which compared the efficacy of tocilizumab—a humanized anti-IL-6 receptor mAb—and MTX for inhibiting the progression of joint destruction [25], the mean TSS of the 306 patients at baseline was 29.4; this figure was extremely high despite the mean disease duration of 2.3 years. The mean estimated yearly progression of TSS for the 306 Japanese RA patients recruited was 13.3, supporting the above hypothesis. In this regard, the lower dose of MTX may be responsible, in part, for the rapid progression of joint destruction, in addition to possible genetic and environmental factors unique to Japanese RA patients.

No significant relationships were noted between the total modified vdH–Sharp score at baseline and most clinical parameters, whereas the total modified vdH–Sharp score was significantly correlated with the disease duration ($r = 0.62$, $P < 0.001$), as confirmed using a multivariate analysis. This conclusion is consistent with the results of a long list of previous reports. Although whether the rate of progression decreases as the disease duration increases continues to be discussed, joint destruction certainly progresses rapidly during the first 1–2 years after disease onset [23, 24]. Our results support the hypothesis that patients with a shorter duration exhibit a higher estimated yearly progression, although this result might reflect our method of calculating progression using the score divided by disease duration since diagnosis of RA, but not initial manifestation [3].

Obviously, structural damage occurs rapidly during the early stage of the disease in caucasian RA patients, and this is also true in Japanese RA patients. The mean estimated yearly progression in patients with early disease was 41.11; this rate was faster than that reported in the PREMIER study, which had the most aggressive structural damage reported so far [26]. In addition, the mean estimated yearly progression in the moderate and advanced RA groups showed similar aggressive features of structural damage in Japanese RA patients, confirming previous results [17].

While we found no unique characteristics among patients with early RA, higher disease activity in patients with moderate RA and a lower doses of MTX in those with advanced RA were correlated with more rapid progression of joint destruction. These results may suggest that patients with distinct disease durations may have different disease features regarding the progression of structural damage. To lessen joint destruction, it is important to realize that infliximab therapy should be started much earlier, before disease activity reaches a high level at which the induction of remission in early RA becomes unlikely. In addition, tight control over disease activity in patients with moderate RA and MTX dose escalation in patients with advanced RA should be seriously considered before starting infliximab therapy.

Compared with the X-ray data at 0 weeks, the effect of infliximab on joint destruction was remarkable in Japanese patients with RA. The change in the total modified vdH–Sharp score was −0.03 out of a full-scale score in the present study, whereas that in the ATTRACT study was 1.3 out of a 440 full-scale score for the arm receiving 3 mg/kg of infliximab every eight weeks. Although 38% of the patients in the present study showed some improvement (whereas 44% of the patients in the 3-mg/kg every eight weeks arm of the ATTRACT study showed improvement), the percentage of patients with major progression was lower in the present study than in the ATTRACT study (1.5 vs. 5.5%). The average reduction from the total score at baseline at 54 weeks after the start of infliximab therapy was 101.14% in the present study, whereas that in the 3-mg/kg every eight weeks arm of the ATTRACT study was 98.35%, indicating a similarly remarkable effect on the suppression of structural damage progression.

Taken together, the present RECONFIRM-2J study demonstrated that joint destruction before the start of infliximab therapy was considerably rapid in Japanese RA patients and confirmed the significant ability of infliximab to halt joint destruction. By analyzing the factors related to joint destruction, we found a significant correlation between disease duration and the TSS at baseline before the start of infliximab therapy. In patients with advanced RA, TSS was negatively correlated with the MTX dose at

0 weeks, while it was significantly correlated with the DAS28 at 0 weeks. However, none of the factors were correlated with joint destruction at 54 weeks after the start of infliximab therapy, suggesting that infliximab remarkably suppressed the progression of structural damage in the vast majority of the patients, irrespective of the clinical characteristics of the patients.

Acknowledgments The authors thank all of the medical staff at the three institutions for providing the data. This work was supported in part by a Research Grant-In-Aid for Scientific Research from the Ministry of Health, Labor and Welfare of Japan.

References

1. Scott DL, Grindulis KA, Struthers GR, Coulton BL, Popert AJ, Bacon PA. Progression of radiological changes in rheumatoid arthritis. Ann Rheum Dis. 1984;43:8–17.
2. Pincus T. Long-term outcomes in rheumatoid arthritis. Br J Rheumatol. 1995;34 Suppl 2:59–73.
3. Scott DL, Pugner K, Kaarela K, Doyle DV, Woolf A, Holmes J, et al. The links between joint damage and disability in rheumatoid arthritis. Rheumatology (Oxford). 2000;39:122–32.
4. Pincus T, Sokka T, Wolfe F. Premature mortality in patients with rheumatoid arthritis: evolving concepts. Arthritis Rheum. 2001;44:1234–6.
5. Doran MF, Pond GR, Crowson CS, O'Fallon WM, Gabriel SE. Trends in incidence and mortality in rheumatoid arthritis in Rochester, Minnesota, over a forty-year period. Arthritis Rheum. 2002;46:625–31.
6. Feldmann M, Brennan FM, Maini RN. Role of cytokines in rheumatoid arthritis. Annu Rev Immunol. 1996;14:397–440.
7. Ivashkiv LB. Cytokine expression and cell activation in inflammatory arthritis. Adv Immunol. 1996;63:337–76.
8. Choy EH, Panayi GS. Cytokine pathways and joint inflammation in rheumatoid arthritis. N Engl J Med. 2001;344:907–16.
9. Feldmann M, Maini RN. Anti-TNF alpha therapy of rheumatoid arthritis: what have we learned? Annu Rev Immunol. 2001;19:163–96.
10. Lipsky PE, van der Heijde DM, St Clair EW, Furst DE, Breedveld FC, Kalden JR, et al. Infliximab and methotrexate in the treatment of rheumatoid arthritis. Anti-tumor necrosis factor trial in rheumatoid arthritis with concomitant therapy study group. N Engl J Med. 2000;343:1594–602.
11. St Clair EW, van der Heijde DM, Smolen JS, Maini RN, Bathon JM, Emery P, et al. Combination of infliximab and methotrexate therapy for early rheumatoid arthritis: a randomized, controlled trial. Arthritis Rheum. 2004;50:3432–43.
12. Taylor PC, Steuer A, Gruber J, McClinton C, Cosgrove DO, Blomley MJ, et al. Ultrasonographic and radiographic results from a two-year controlled trial of immediate or one-year-delayed addition of infliximab to ongoing methotrexate therapy in patients with erosive early rheumatoid arthritis. Arthritis Rheum. 2006;54:47–53.
13. Abe T, Takeuchi T, Miyasaka N, Hashimoto H, Kondo H, Ichikawa Y, et al. A multicenter, double-blind, randomized, placebo controlled trial of infliximab combined with low dose methotrexate in Japanese patients with rheumatoid arthritis. J Rheumatol. 2006;33:37–44.
14. Takeuchi T, Tatsuki Y, Nogami Y, Ishiguro N, Tanaka Y, Yamanaka H, et al. Post-marketing surveillance of the safety profile of infliximab in 5,000 Japanese patients with rheumatoid arthritis. Ann Rheum Dis. 2008;67:189–94.
15. Yamanaka H, Tanaka Y, Sekiguchi N, Inoue E, Saito K, Kameda H, et al. Retrospective clinical study on the notable efficacy and related factors of infliximab therapy in a rheumatoid arthritis management group in Japan (RECONFIRM). Mod Rheumatol. 2007;17:28–32.
16. Tanaka Y, Takeuchi T, Inoue E, Saito K, Sekuguchi N, Iikuni N, et al. Retrospective clinical study on the notable efficacy and related factors of infliximab therapy in a rheumatoid arthritis management group in Japan: 1-year clinical and ragiographic outcomes (RECONFIRM-II). Mod Rheum. 2008;18:146–152.
17. Kameda H, Sekiguchi N, Nagasawa H, Amano K, Takei H, Suzuki K, et al. Development and validation of handy rheumatoid activity score with 38 joints (HRAS38) in rheumatoid arthritis patients receiving infliximab. Mod Rheumatol. 2006;16:381–8.
18. Arnett FC, Edworthy SM, Bloch DA, McShane DJ, Fries JF, Cooper NS, et al. The American rheumatism association 1987 revised criteria for the classification of rheumatoid arthritis. Arthritis Rheum 1988;31:315–24.
19. Miyasaka N, Takeuchi T, Eguchi K. Proposed [corrected] Japanese guidelines for the use of infliximab for rheumatoid arthritis. Mod Rheumatol. 2005;15:4–8.
20. Inoue E, Yamanaka H, Hara M, Tomatsu T, Kamatani N. Comparison of disease activity score (DAS)28– erythrocyte sedimentation rate and DAS28– C-reactive protein threshold values. Ann Rheum Dis. 2007;66:407–9.
21. van der Heijde D, Lassere M, Edmonds J, Kirwan J, Strand V, Boers M. Minimal clinically important difference in plain films in RA: group discussions, conclusions, and recommendations. OMERACT imaging task force J Rheumatol. 2001;28:914–7.
22. Maini RN, Breedveld FC, Kalden JR, Smolen JS, Furst D, Weisman MH, et al. Sustained improvement over two years in physical function, structural damage, and signs and symptoms among patients with rheumatoid arthritis treated with infliximab and methotrexate. Arthritis Rheum. 2004;50:1051–65.
23. Strand V, Landewe R, van der Heijde D. Using estimated yearly progression rates to compare radiographic data across recent randomised controlled trials in rheumatoid arthritis. Ann Rheum Dis. 2002;61(suppl 2):ii61–4.
24. Wick MC, Anderwald C, Weiss RJ, Imhof H, Kainberger F, Smolen JS. Radiological progression of joint damage in a longitudinal cohort of early DMARD-treated rheumatoid arthritis patients followed for 10 years. Scand J Rheumatol. 2004;33:162–6.
25. Nishimoto N, Hashimoto J, Miyasaka N, Yamamoto K, Kawai S, Takeuchi T, et al. Study of active controlled monotherapy used for rheumatoid arthritis, an IL-6 inhibitor (SAMURAI): evidence of clinical and radiographic benefit from an X-ray reader-blinded randomised controlled trial of tocilizumab. Ann Rheum Dis. 2007;66:1162–7.
26. Breedveld FC, Weisman MH, Kavanaugh AF, Cohen SB, Pavelka K, van Vollenhoven R, et al. The PREMIER study: a multicenter, randomized, double-blind clinical trial of combination therapy with adalimumab plus methotrexate versus methotrexate alone or adalimumab alone in patients with early, aggressive rheumatoid arthritis who had not had previous methotrexate treatment. Arthritis Rheum. 2006;54:26–37.

International Immunology, Vol. 20, No. 11, pp. 1427–1437
doi:10.1093/intimm/dxn100

© The Japanese Society for Immunology. 2008. All rights reserved.
For permissions, please e-mail: journals.permissions@oxfordjournals.org

Impaired TCR signaling through dysfunction of lipid rafts in sphingomyelin synthase 1 (*SMS1*)-knockdown T cells

Zhe-Xiong Jin[1], Cheng-Ri Huang[1], Lingli Dong[1,2], Seiji Goda[3], Takafumi Kawanami[1], Toshioki Sawaki[1], Tomoyuki Sakai[1], Xiao-Peng Tong[1], Yasufumi Masaki[1], Toshihiro Fukushima[1], Masao Tanaka[1], Tsuneyo Mimori[4], Hiromasa Tojo[5], Eda T. Bloom[6], Toshiro Okazaki[7] and **Hisanori Umehara[1]**

[1]Department of Hematology and Immunology, Kanazawa Medical University, 1-1 Daigaku, Uchinada, Ishikawa 920-0293, Japan
[2]Department of Hematology and Immunology, Tongji Hospital, Huazhong University of Science and Technology, Wuhan, Hubei 430030, China
[3]Department of Biochemistry, Osaka Dental University, Kuzuha, Osaka, Japan
[4]Department of Rheumatology and Clinical Immunology, Kyoto University Graduate School of Medicine, Sakyo-ku, Kyoto 606-8507, Japan
[5]Department of Biochemistry and Molecular Biology, Osaka University Graduate School of Medicine, Osaka 565-0871, Japan
[6]Division of Cellular and Gene Therapies (HFM-725), Center for Biologics Evaluation and Research, Food and Drug Administration, Bethesda, MD 20892, USA
[7]Department of Clinical Laboratory, Medicine/Hematology, Faculty of Medicine, Tottori University, Yonago, Tottori 683-8504, Japan

Keywords: LAT, lipid rafts, microdomain, sphingomyelin, TCR

Abstract

During T cell activation, TCRs cluster at the center of the T cell–antigen-presenting cell interface forming the central supramolecular activation cluster. Although it has been suggested that sphingolipid- and cholesterol-rich microdomains, termed lipid rafts, form platforms for the regulation and transduction of TCR signals, an actual role for membrane sphingomyelin (SM), a key component of lipid rafts, has not been reported. After cloning a gene responsible for SM synthesis, sphingomyelin synthase (SMS) 1, we established a SM-knockdown cell line (Jurkat-SMS1/kd) by transfection of SMS1-short-interfering RNA into Jurkat T cells, which is deficient in membrane expression of SM. Upon CD3 stimulation, expression of CD69 (the earliest leukocyte activation antigen), activation-induced cell adhesion and proliferation as well as TCR clustering was severely impaired in Jurkat-SMS1/kd cells. CD3-induced tyrosine phosphorylation and association of linker for activation of T cell with *ZAP-70* and Grb2 and phosphorylation of protein kinase C (PKC) θ were also severely impaired in Jurkat-SMS1/kd cells. Finally, translocation of TCR, *ZAP-70* and PKCθ into lipid rafts was markedly decreased in Jurkat-SMS1/kd cells. These findings indicate that membrane SM is crucial for TCR signal transduction, leading to full T cell activation through lipid raft function.

Introduction

Sphingolipid- and cholesterol-rich microdomains, termed lipid rafts, play a key role in protein sorting (1). They have been implicated in the cytoskeletal re-organization that forms platform immunological synapses at the cell membrane, which are involved in signal transduction, for example of signals originating through the TCR (2–4). Since the lipid raft-resident molecules such as *src* family kinases and ganglioside GM1 relocalize toward the immunological synapse, it appears that the immunological synapse could be described as a merger of lipid rafts (5, 6).

The stimulation on TCR and CD3 complexes induces a series of signal transduction events leading to activation of cytosolic protein tyrosine kinases (PTKs) such as *lck* and *ZAP-70*. Activated *ZAP-70* phosphorylates the transmembrane adaptor protein linker for activation of T cells (LATs). LAT consists of primarily cytoplasmic region with two cysteine residues

Correspondence to: H. Umehara; E-mail: umehara@kanazawa-med.ac.jp

Transmitting editor: K. Okumura

Received 28 June 2008, *accepted* 11 August 2008

Advance Access publication 26 September 2008

just below the transmembrane region and is targeted to lipid rafts by palmitoylation of cysteines (7). Tyrosine phosphorylated LAT, via phosphotyrosine-based docking motifs, recruits SH2 domain-containing signaling proteins, including SLP-76, phospholipase Cγ (PLCγ), phosphatidylinositol 3 kinase (PI3K) and Grb2 etc., and allows subsequent extension of the signaling scaffold (8).

Another important pathway for T cell activation different from tyrosine kinase cascade is the signal scaffolding of CARMA1 (caspase recruitment domain, CARD, membrane-associated guanylate kinase, MAGUK, protein 1) and translocation of protein kinase C (PKC) θ into lipid rafts. Among the PKC isoforms, PKCθ, a Ca^{2+}-independent PKC isoform, is a critical component for TCR-induced NF-κB activation, because mice deficient for PKCθ show impaired activation of NF-κB (9), and PKCθ is selectively expressed in T cells and translocates to lipid rafts during antigen-receptor triggering (10). Taken together, these data support an important role for lipid rafts in TCR-mediated protein sorting and signal transduction.

In addition to these biochemical events, lipid rafts are implicated in the formation of the immunological synapse, where spatial organization and compartmentalization of membrane-associated proteins such as the TCR–CD3 complex, PTKs and adaptor molecules occur (8, 11). Immunological synapse formation with the central supramolecular activation cluster (cSMAC) depends on TCR-mediated signaling that induces the re-organization of the cytoskeleton and cell surface receptors, and the immunological synapse mediates effector functions. However, recent imaging analyses such as single-particle tracking, fluorescence resonance energy transfer (FRET) microscopy, FRET microscopy with fluorescence recovery after photobleaching and total internal reflection fluorescence microscopy reveal that TCR microclusters form prior to immunological synapses, are the site for antigen recognition and T cell activation and are continuously generated at the periphery of immunological synapses but are not accompanied by lipid raft clustering (12–14). Thus, the functional roles of the immunological synapses and lipid rafts for the spatial-temporal organization of the enzymatic events during signaling are controversial.

Lipid rafts have been detected using cholera toxin B (CTx) which binds to ganglioside GM1 co-localized in rafts, and the role of rafts has been evaluated by disruption of rafts using the cholesterol-chelating reagent, methyl-β-cyclodextrin (MβCD). However, there has been no direct evidence that membrane sphingomyelin (SM) is involved in raft functions and TCR-mediated signal transduction due to the lack of molecular cloning of the sphingomyelin synthase (SMS) gene and of a specific probe to membrane SM. Previously, we and others have succeeded in cloning the human cDNA for *SMS1* (15, 16). Using SM synthesis-deficient cells and cells in which function has been restored by transfection with *SMS1* gene, we have reported that membrane SM plays a key role in Fas-mediated apoptosis through its involvement in the efficient clustering of Fas and lipid rafts (17).

We herein report the establishment of a membrane SM-deficient cell line (Jurkat-SMS1/kd) by transfection of SMS1-short-interfering RNA (siRNA) into Jurkat T cells, and provide data demonstrating the role of membrane SM on T cell functions and CD3-activated signal pathways.

Methods

Antibodies and reagents

The human CD3ε-specific mAb, OKT3 (IgG_{2a}), was purchased from Biodesign International a custom ascites. The antibodies to anti-PKCθ, anti-Grb2, anti-LAT, anti-*lck*, anti-TCRβ and FITC-conjugated goat anti-rabbit IgG2a were purchased from Santa Cruz Biotechnology. Anti-phospho-PKCθ (Thr538) was purchased from Cell Signaling Technology (Beverly, MA, USA). Anti-TCRβF1 antibody was purchased from PIERCE ENDOGEN a Perbio Science (Rockford, IL, USA), anti-*ZAP-70* and anti-phosphotyrosine (4G10) antibody were purchased from Upstate Cell Signaling (Lake Placid, NY, USA). Rabbit anti-MBP anti-serum was purchased from New England BioLabs (Beverly, MA, USA). PE-conjugated anti-human CD2, CD3, CD4, CD69, CD95 and anti-human TCRαβ antibody were purchased from BD Bioscience (San Jose, CA, USA). Lysenin, goat anti-mouse IgG, FITC-conjugated CTx, HRP-conjugated CTx, PE-conjugated rabbit anti-mouse IgG, FITC-conjugated anti-rabbit IgG were purchased from Sigma–Aldrich (St Louis, MO, USA). The cell viability assay kit (WST-8) was purchased from Wako Co. Ltd (Kyoto, Japan). L-[U-^{14}C] serine was purchased from Amersham Biosciences (Piscataway, NJ, USA). The ECL immunodetection system, HRP-conjugated goat anti-mouse and anti-rabbit IgG mAb were obtained from Amersham International (Amersham, Bucks, UK).

Construction of human SMS1-siRNA vector

The sequences of siRNA for human *SMS1* genes and the control (scrambled sequence (SCR)) were designed by siRNA Design Support System (Takara Bio, Shiga, Japan). The sequences are as follows: *SMS1*, GCCCAACTGCGAAGAATAA (seq. #6) and SCR, ATTGAAAAAGACACGCGCC (temporally designated SMS negative). Based on these sequences, 'top (T)' and 'bottom (B)' pairs of oligonucleotides were synthesized as follows: *SMS1*-RNAi6-T (for *SMS1*), GATCCGCCCAACTGCGAAGAATAATTCAAGAGATTATTCTTCGCAGTTGGGCTTTTTTAT; *SMS1*-RNAi6-B (for *SMS1*), CGATAAAAAAGCCCAACTGCGAAGAATAATCTCTTGAATTATTCTTCGCAGTTGGGCG; SMSneg-RNAi-T (for SCR), GATCCATTGAAAAAGACACGCGCCTTCAAGAGAGGCGCGTGTCTTTTTCAATTTTTTTAT and SMSneg-RNAi-B (for SCR), CGATAAAAAATTGAAAAAGACACGCGCCTCTCTTGAAGGCGCGTGTCTTTTTCAATG. The 'T' and 'B' pairs of oligonucleotides were annealed and ligated into *Bam*HI and *Cla*I sites of pSINsi-hU6 (Takara Bio) according to the manufacturer's instruction. The ligation was confirmed by digestion with *Bam*HI and *Bln*I (performed 40127-40129 and 40330 for *SMS* and SCR, respectively). The resultant vectors were designated pSINsi-*SMS1* and SCR, respectively, and transfected into Jurkat T cells via retroviral particles.

Cell transfection and establishment of SM-knockdown Jurkat T cells

Production of the retrovirus carrying the *SMS1*-siRNA and SCR-siRNA as well as infection by the recombinant viruses were performed as previously reported (18). Cells were selected with 1–3 mg ml^{-1} G418 for several weeks and then

separated into single cells by limiting dilution. The isolated clones showing the most suppression of *SMS1* level (Jurkat-SMS1/kd) and control (Jurkat-SM+) were chosen for further experiments.

Measurement of the SMS1-expression level by real-time PCR

Total RNA was isolated from Jurkat-SM+ and Jurkat-SMS1/kd cells using QIAGEN RNeasy kit (QIAGEN, MD, USA) and the cDNA was synthesized using first-strand cDNA synthesis kit (Life Sciences). Open reading frame sequences of SMS cDNA were amplified using Pyrobest DNA polymerase (Takara Bio) and primers *SMS1*-F4 (TGTCCTGCCAAGAGAGAGC) and *SMS1*-R1 (TGGAGTTCTTAGCACTTCGG) for *SMS1* (PCR performed: 40311), *SMS2*-F5 (ACAAGAACTTGACCATCTCC) and *SMS2*-R4 (TTGCTCCTCAGGTCGATTTC) for *SMS2* (PCR performed: 40122) and *SMS3*-F2 (AGCTGAGGCTGAGGAGAG) and *SMS3*-R4 (CATCCAATTAGTCTTTTCATTATTG) for *SMSr* (PCR performed: 40122). As a control, human glyceraldehyde 3-phosphate dehydrogenase (GAPDH) mRNA was analyzed using primers GAPDH-F (CAACGGATTTGGTCGTATT, upstream) and GAPDH-R (CACAGTCTTCTGGGTGGC, downstream). In 2 μl of the synthesized DNA, 2 premix (10 μl), up- and downstream primers of GAPDH (1 μl of each) were added sequentially, with the total volume adjusted to 20 μl with triple distilled water. The mixture was loaded in a 7500 real-time PCR system (Applied Biosystem) and pre-denaturation at 94°C for 5 min, 35 cycles of denaturation at 94°C for 30 s, annealing at 55°C for 30 s and extension at 72°C for 30 s were carried out, followed by a final extension at 72°C for 7 min. The PCR (real-time form) production of the DNA copy base pairs was computed by Avogadro's number system.

FACS analyses

To detect SM localized at the outer leaflet of the plasma membrane, cells were stained on ice for 30 min with non-toxic lysenin fused to maltose-binding protein (MBP-lysenin) (19), followed with rabbit anti-MBP anti-serum (New England BioLabs) and FITC-conjugated anti-rabbit IgG (Sigma-Aldrich) and analyzed with a FACS Calibur (Becton Dickinson, Mountain View, CA, USA). Surface expressions of ganglioside GM1 and cholesterol were analyzed using FITC-conjugated CTx (Sigma-Aldrich) and a fluorescein ester of poly(ethyleneglycol)-derivatized cholesterol ether (fPEG-Chol) (20), respectively. Data were analyzed using Cell Quest software (Becton Dickinson).

Confocal microscopy

For visualization of SM localized at the outer leaflet of plasma membrane, cells were allowed to settle onto slides coated with poly-L-lysine, fixed in 4% formaldehyde, stained with lysenin-MBP at 4°C for 20 min, followed with anti-MBP mAb and FITC-conjugated anti-mouse IgG mAb. Cells were also stained with PE-conjugated anti-human αβTCR antibody or FITC-conjugated CTx subunit. Fluorescence was detected with a confocal microscope (Zeiss LSM-5 Pascal laser scan, Carl Zeiss, Oberkochen, Germany) equipped (21).

To assess the co-localization of TCR, SM and ganglioside GM1, cells were stained with 5 μg ml^{-1} of anti-CD3 antibody (OKT3) at 4°C for 15 min. After washing, cells were warmed up to 37°C in a water bath and cross-linked with 10 μg ml^{-1} of anti-mouse IgG antibody for 5 min. Cells were fixed with 4% paraformaldehyde for 20 min at 22 °C and mounted in FITC-conjugated secondary antibody. Large clusters of TCR were defined as cells in which the fluorescence condenses onto >25% of the cell surface, whereas fluorescence was homogenously distributed on the membrane of non-stimulated cells. In each experiment, a blinded observer counted 150–200 cells, and a second independent observer confirmed the count.

Cell adhesion and migration assays

Adhesion and migration assays with Jurkat-SMS1/kd and Jurkat-SM+ cells were performed using calcein-acetoxymethyl ester labeling of cells described as previously (22). Adhesion assays were performed in flat-bottomed 96-well plates (Costar, Cambridge, MA, USA) pre-coated with 0.3 μg per well fibronectin (FN) and blocked with PBS supplemented with 2.5% BSA (23). Cells were re-suspended in PBS supplemented with 0.5% human serum albumin (PBS/HSA) at 1.6×10^6 cells ml^{-1} after Ficoll separation. For CD3 stimulation, cells were pre-incubated on ice for 30 min with OKT3 mAb and then washed twice with PBS/HSA. After washing, 80 000 cells per well were added to the appropriate wells. The following stimulating agents were added to the wells before the addition of cells: 10 ng ml^{-1} phorbol myristate acetate (PMA) or 1 μg ml^{-1} of goat anti-mouse IgG (for CD3 stimulation). Cells were incubated at 4°C for 1 h, plates were floated in a 37°C water bath for the indicated times and non-adherent cells were removed by washing and fluorescence was measured as described previously (24).

Migration assays were performed in transwell chambers with 3-mm polycarbonate membrane (Corning Incorporated) pre-coated with 100 μg ml^{-1} FN or inter cellular adhesion molecules-1 (ICAM-1) on both sides of the filter. Human stromal cell-derived factor 1α (CXCL12) was diluted to appropriate concentrations in medium and added to the lower chamber of the transwell chambers. The cells were allowed to migrate for 4 h at 37°C in 5% CO_2. Each sample was assayed in triplicate, and migrated cells were counted in five randomly selected high-power fields (×400) per well. Results were expressed as mean ± SD per mm^2 from one representative experiment.

Cell labeling, lipid separation and ceramide measurement

For detection of SM synthesis, cells were re-seeded at 5×10^5 cells ml^{-1} in the RPMI-1640 medium with 2% FBS and L-[^{14}C] serine (specific activity; 155 mCi $mmol^{-1}$) and incubated at 37°C in 5% CO_2 for 36 h. The cell lipids were extracted, applied to silica gel thin-layer chromatography (TLC) plates (Whatman, Maidstone, UK) and developed as described previously (25). Radioactivity within spots of ceramide-1-phosphate was estimated with a BASE III image analyzer system (Fuji Photo Film, Kanagawa, Japan) and expressed as photo-stimulated luminescence arbitrary units (26).

HPLC/mass spectrometric analysis

To assess the amounts and molecular species compositions of SM in the *SMS1*-deficient cells, we used normal-phase

HPLC/ion-trap mass spectrometry (27, 28). Lipid extracts were prepared from cell pellets supplemented with appropriate amounts of myristoyl ceramide, lauroyl glucosylceramide, lauroyl lactosylceramide and lauroyl SM as internal standards, evaporated under N_2 and dissolved in hexane/2-propanol (3:2). To remove the majority of ester-containing lipids, an aliquot was hydrolyzed at a mild alkaline pH and 60°C for 60 min, extracted by the Bligh and Dyer method, evaporated and finally dissolved in the previous solvent. An aliquot (1–2 μl) of the extracts was directly subjected to HPLC/mass spectrometry. Sphingolipids were separated into their classes and subclasses in the order from lower to higher polarity on a trap and separation silica columns connected in series (Fortispack of 1–20 mm and 1–100 mm, OmniSeparo-TJ, Inc., Hyogo, Japan). Effluents were monitored with an LCQdeca-XP mass spectrometer interfacing with an XYZ stage equipped with a fluoropolymer-coated electrospray tip, FortisTip (OmniSeparo-TJ, Inc.) of 150 μm in outer diameter/20 μm in inner diameter. Sphingolipids were identified with the mass-to-charge ratio (*m/z*) values and data-dependent, first or second-stage tandem mass spectrometry (MS/MS or MS^3) and quantified based on comparison of peak areas on chromatograms of target and internal standard ions of the same class. Peak area values were corrected for the contributions of natural abundance ^{13}C isotope, i.e. the difference between the carbon numbers of a target and an internal standard molecule and the overlapping of ions with 2 ^{13}C isotopes replaced in molecular ions with 2-amu lower mass (29).

Immunoprecipitation, western blotting and immunoblotting

Cells were solubilized with lysis buffer containing 50 mM Tris–HCl, pH 7.6, 1% Brij 97, 300 mM NaCl, 5 mM EDTA, 10 μg ml^{-1} leupeptin, 10 μg ml^{-1} aprotinin, 1 mM phenylmethylsulfonyl fluoride (PMSF) and 1 mM sodium orthovanadate with gentle rocking for 30 min at 4°C. Immunoprecipitated proteins were fractionated by SDS–PAGE (8–12% polyacrylamide gels), electrophoretically transferred to membranes and blotted with antibodies as indicated. Peroxidase-conjugated secondary antibodies (Amersham) were used at a 1:1000 dilution and immunoreactive bands were visualized using ECL (Amersham) (26). Densitometry of the protein bands was performed using NIH image software (30). Quantitation of bands was corrected to the density of ganglioside GM1 and depicted as arbitrary units.

Isolation of a raft fraction in equilibrium density gradients

Raft fractions from 2.5 × 10^8 cells were prepared as described by Rodgers and Rose with minor modifications (21). In brief, 2.5 × 10^8 cells were lysed with 0.8 ml MS-buffered saline (MBS; 25 mM MES, pH 6.5, and 150 mM NaCl) containing 1% Triton X-100, 10 μg ml^{-1} leupeptin, 10 μg ml^{-1} aprotinin, 1 mM PMSF, 1 mM sodium orthovanadate and 5 mM EDTA. The lysate was homogenized with 10 strokes of a Dounce homogenizer (IWAKI Glass Co.), gently mixed with an equal volume of 80% sucrose (wt/vol) in MBS and placed in the bottom of a 14 × 89 mm clear centrifuge tube (model 344096; Beckman Coulter). The sample was then overlaid with 5.2 ml of 30% sucrose and 2.8 ml of 5% sucrose in MBS and centrifuged at 41 000 r.p.m. (rotor model SW41Ti; Beckman Coulter, Palo Alto, CA, USA) at 4°C for 21 h. After centrifugation, twelve 0.8-ml fractions (excluding the pellet) were collected from the top of the gradient. To examine the presence of cell surface and intracellular proteins in the density gradient fractions, 20 μl of each fraction was separated by SDS–(10–12%) PAGE and transferred to immobilon polyvinylidene difluoride membranes (Millipore, Bedford, MA, USA) for standard western blot analysis.

Assay for SMS activity

SMS1 activity assays were performed as described previously (15). Briefly, cells were homogenized in an ice-cold buffer containing 20 mM Tris–HCl, pH 7.4, 2 mM EDTA, 10 mM EGTA, 1 mM PMSF and 2.5 μg ml^{-1} leupeptin. The lysates containing 500 μg of cell protein were added to a reaction solution containing 10 mM Tris–HCl, pH 7.5, 1 mM EDTA, 20 μM C6-NBD-ceramide, 120 μM phosphatidyl choline and incubated at 37°C for 30 min. The lipids were extracted by the method of Bligh and Dyer, applied on the TLC plates and developed with solvent containing chloroform/methanol/12 mM $MgCl_2$ in H_2O (65:25:4) (31). The fluorescent lipids were visualized with a FluoroImager SI system (Amersham Biosciences). The radioactive spots were visualized using the BAS 2000 system.

Results

Establishment of membrane SM-knockdown cells (Jurkat-SMS1/kd)

After cloning the human cDNA-encoding *SMS1* (15), we established membrane SM-knockdown cell lines (Jurkat-SMS1/kd) and control cell lines (Jurkat-SM+) by transfection of Jurkat cells with *SMS1*- or control siRNAs followed by selection with geneticin and limiting dilution.

To examine the expression levels of *SMS1* gene in Jurkat-SMS1/kd and Jurkat-SM+ cells, we isolated total RNA from each cell line, and sense/anti-sense oligonucleotides for *SMS1*, *SMS2*, *SMSr* and GAPDH cDNAs were utilized to perform RT-PCR and real-time PCR. Results revealed that *SMS1* was a major SMS gene in Jurkat cells and that *SMS1* gene copy number was decreased in the Jurkat-SMS1/kd cells to ~60% of Jurkat-SM+ cells (Fig. 1A). To detect SMS1 enzyme activity, lipids were extracted from each cell lysates, and ceramide mass measurement was performed by diacylglycerol kinase assay (25). The enzyme activity in Jurkat-SMS1/kd cells was decreased to ~60% of that in Jurkat-SM+ cells (Fig. 1B). We next examined the overall lipid composition of Jurkat-SMS1/kd and Jurkat-SM+ cells using HPLC and mass spectrometric analysis. Jurkat-SMS1/kd cells displayed only a minor (up to 23%) reduction in SM levels compared with Jurkat-SM+ cells, namely 2.8 versus 3.6 nmol mg^{-1} protein (Fig. 1C). Jurkat cells contain limited numbers of SM molecular species, such as C16:0, C16:1, C22:0, C24:0 and C24:1, where the symbols indicate the carbon number followed by a colon and the number of double bonds in the acyl group. SMS1 deficiency in Jurkat cells did not change the molecular species distribution in SM so much (Fig. 1C).

Lysenin is a SM-directed cytolysin purified from the earthworm, which specifically binds to membrane SM and

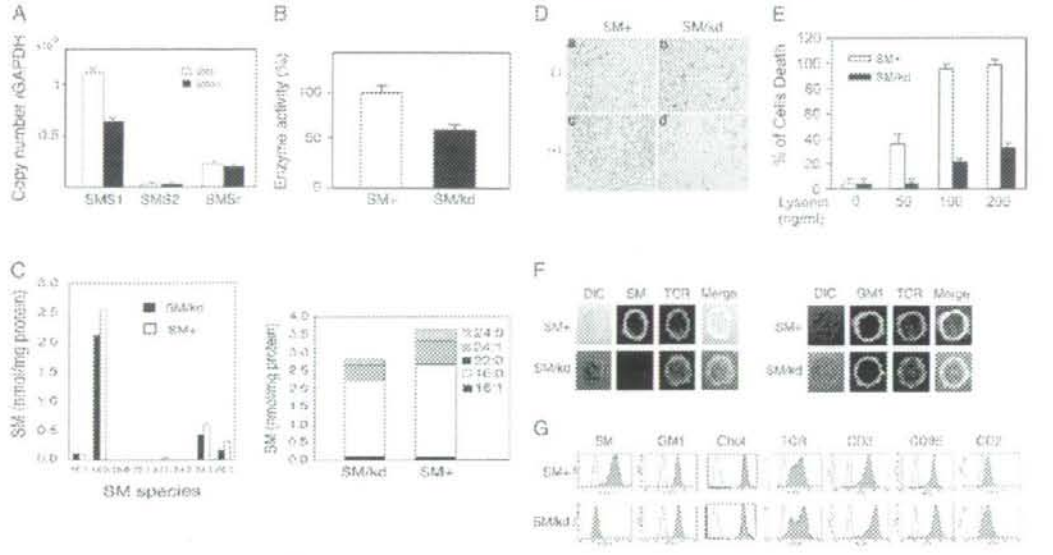

Fig. 1. SM-knockdown cells. (A) The *SMS1* gene expression. Expression levels of *SMS* genes were examined by RT–PCR and real-time PCR in Jurkat-SM+ and Jurkat-SMS1/kd cells. Each copy number was corrected to those of GAPDH. Results are representative of three experiments. (B) SMS1 enzyme activity in Jurkat-SM+ and Jurkat-SMS1/kd cells. Lipids were extracted from each cell lysate, and ceramide mass measurement was performed by the diacylglycerol kinase assay. Results are representative of three experiments. (C) Amounts of SM. Cell lipid extracts were prepared and subjected to liquid chromatography and electrospray ionization tandem MS as described under Methods. SM+, Jurkat-SM+ cells; SM/kd, Jurkat-SMS1/kd cells. (D) Microscopy of cells exposed to lysenin. Jurkat-SM+ cells (a and c) and Jurkat-SMS1/kd cells were treated in the presence (c and d) or absence (a and b) of 100 ng ml^{-1} of lysenin at 37 °C for 1 h and stained with 1% trypan blue. (E) Sensitivity against lysenin-mediated cell lysis. Cells were treated with the indicated concentration of lysenin at 37 °C for 1 h, then stained PI (propidium iodide) and analyzed by FACS scan. SM+, Jurkat-SM+ cells; SM/kd, Jurkat-SMS1/kd cells. Data are representative of three independent experiments. (F) Analysis of membrane SM expression by confocal microscopy. Cells were stained with lysenin-MBP and FITC-conjugated anti-mouse IgG mAb, PE-conjugated anti-TCR mAb or FITC-conjugated CTx. DIC, differential interference contrast; GM1, ganglioside GM1. (G) FACS analysis of membrane SM. To detect membrane SM, cells were stained with lysenin-MBP and FITC-conjugated anti-mouse IgG mAb. Surface expressions of ganglioside GM1 and cholesterol were analyzed using FITC-conjugated CTx and fPEG-Chol, respectively. Surface markers were analyzed with PE-conjugated anti-TCR, CD3, CD95 and CD2 mAbs. SM+, Jurkat-SM+ cells; SM/kd, Jurkat-SMS1/kd cells. Data are representative of more than five independent experiments.

induces pore formation in the plasma membrane and subsequent cell death (32, 33). We next examined the sensitivity to lysenin of Jurkat-SMS1/kd and Jurkat-SM+ cells (Fig. 1D). Cells were treated with 0, 50, 100 and 200 ng ml^{-1} of cytotoxic lysenin in the presence of 20 μg ml^{-1} of propidium iodide at room temperature for 15 min, and cell viability was analyzed with FACS. The results showed that Jurkat-SM+ cells underwent cell death after lysenin treatment in a dose-dependent manner with ~100% cell death at 100 ng ml^{-1} of lysenin, while Jurkat-SMS1/kd cells showed strong resistance (Fig. 1E).

Kiyokawa *et al.* (34) produced non-toxic lysenin by deleting N-terminal amino acids, which specifically binds to SM without induction of cell death. Using the mutant lysenin conjugated with MBP-lysenin, we examined the expression of membrane SM as well as expression of TCR on Jurkat-SMS1/kd and Jurkat-SM+ cells by confocal microscopy. Expression of TCR and ganglioside GM1, which is detected by CTx subunit and considered as a marker of lipid rafts, was detected equivalently on both cells. However, membrane SM was detected only on the surface of Jurkat-SM+ cells, but not on Jurkat-SMS1/kd cells (Fig. 1F). Next, we examined the expression of surface receptors and other membrane components such as CD3, CD95/Fas, CD2, αβTCR, ganglioside GM1 as well as membrane SM by FACS analysis. Membrane cholesterol partition was analyzed using fluorescein ester of fPEG-Chol as a probe (20). All markers except membrane SM were expressed at similar levels on both Jurkat-SMS1/kd and Jurkat-SM+ cells (Fig. 1G).

Role of membrane SM in clustering of TCR and lipid rafts

T cell stimulation induces formation of a large, multicomponent complex at the site of contact between T cells and antigen-presenting cell, termed the supramolecular activation complex or the immunological synapse (11, 35). This contact area of the T cell is highly enriched in lipid rafts or microdomains (5, 36). We examined the TCR clustering and co-localization with lipid rafts in Jurkat-SMS1/kd and Jurkat-SM+ cells using confocal microscopy. Full clustering of TCR and co-localization with TCR/lipid rafts were observed in Jurkat-SM+ cells after CD3 activation, but clustering in Jurkat-SMS1/kd cells was impaired (Fig. 2A) or diminished

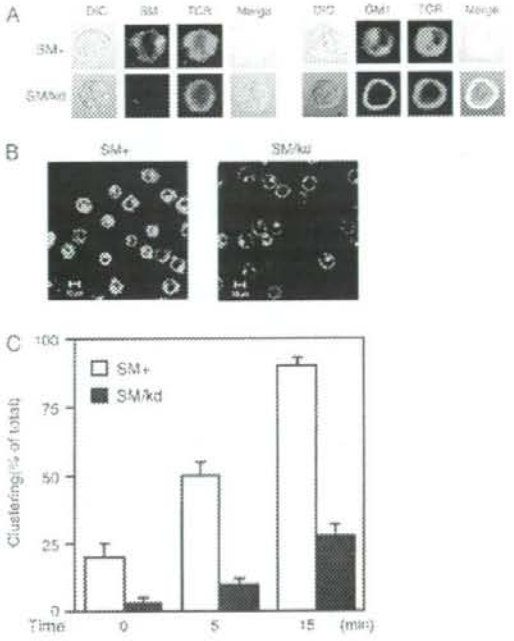

Fig. 2. Role of membrane SM in clustering of TCR and lipid rafts. (A) Confocal microscopy of membrane components after CD3 stimulation. Cells were stimulated with 5.0 μg ml^{-1} of CD3 mAb for 5 min and fixed with 1% paraformaldehyde for 10 min and fixed cells were incubated with FITC-labeled CTx (GM1), PE-conjugated anti-TCR and lysenin-MBP with FITC-conjugated anti-MBP (SM). (B) Confocal microscopy of TCR clustering. Cells were stimulated with 5.0 μg ml^{-1} of CD3 mAb for 5 min and fixed cells were incubated with FITC-conjugated anti-TCR. (C) Time kinetic study of TCR clustering. Cells were stimulated with 5.0 μg ml^{-1} of CD3 mAb for the indicated time and fixed cells were incubated with FITC-conjugated anti-TCR. Large clusters of TCR were defined as cells in which the fluorescence condenses onto >25% of the cell surface, whereas fluorescence was homogenously distributed on the membrane of non-stimulated cells. These data are representative of three independent experiments.

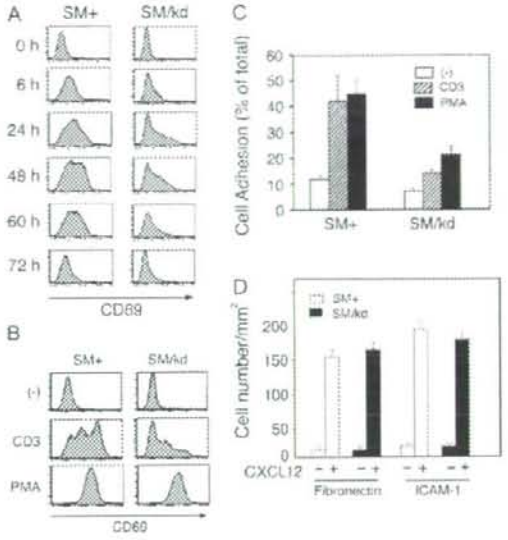

Fig. 3. Roles of membrane SM on CD3-mediated T cell activation. (A) Time kinetics of CD69 expression after CD3 stimulation. Cells were stimulated with 1 μg ml^{-1} of anti-CD3 mAb (OKT3) for the indicated time, and expression of CD69 was analyzed by FACS. (B) Effect of PMA on CD69 expression. Cells were stimulated with 1 μg ml^{-1} of OKT3 mAb or 2 ng ml^{-1} of PMA for 24 h and then expression of CD69 was assessed using FACS scan. (C) Cell adhesion to FN. Cells were labeled with calcein-acetoxymethyl ester. After CD3 activation or PMA stimulation, adhesion assays were performed in flat-bottomed 96-well plates pre-coated with 0.3 μg per well of FN. Data are expressed as % of total applied cells. (D) Cell migration to CXCL12. Migration assays were performed in transwell chambers pre-coated with 100 μg ml^{-1} FN or ICAM-1. After 4 h, migrated cells were counted in five randomly selected high power fields (×400) per well. Results were expressed as mean ± SD per mm^2 from one representative experiment. Results are representative of three independent experiments for (A), (B) and (C), respectively. SM+, Jurkat-SM+ cells; SM/kd, Jurkat-SMS1/kd cells.

in size even though TCR were clustered (Fig. 2B). A time course study showed that TCR/rafts clustering in Jurkat-SM+ cells were 62 and 90% for 5 and 15 min, respectively, and that those in Jurkat-SMS1/kd cells were 15 and 30%, respectively (Fig. 2C). These results indicate that TCR/rafts clustering was severely impaired in Jurkat-SMS1/kd cells compared with Jurkat-SM+ cells.

Roles of membrane SM in CD3-mediated T cell activation

To address our hypothesis that membrane SM has a role in T cell activation, cells were stimulated with 1 μg ml^{-1} of anti-CD3 mAb (OKT3) for 6, 24, 48, 60 and 72 h, and cellular expression of CD69, the earliest leukocyte activation marker (37), was analyzed by FACS. CD69 expression on Jurkat-SMS1/kd cells was markedly decreased over the time course of the assay compared with that on Jurkat-SM+ cells (Fig. 3A). We also examined the effect of PMA, a direct PKC activator, on expression of CD69 in Jurkat-SMS1/kd and Jurkat-SM+ cells. Although CD69 expression induced by CD3 cross-linking was markedly decreased in Jurkat-SMS1/kd cells, similar levels of CD69 were induced by PMA on both cell types (Fig. 3B). These results suggest that membrane SM is involved in TCR/CD3-mediated CD69 expression.

Activation of T cells through the CD3–TCR complex or phorbol esters results in a rapid increase of cell adhesion through integrin receptor activation (24, 38). Therefore, we examined adhesion of Jurkat-SMS1/kd and Jurkat-SM+ cells to FN after CD3/TCR activation or PMA stimulation. As shown in Fig. 3(C), CD3 cross-linking as well as PMA stimulation dramatically enhanced adhesion of Jurkat-SM+ cells to FN compared with only a marginal increase in Jurkat-SMS1/kd cells. We also examined migration of Jurkat-SMS1/kd and Jurkat-SM+ cells in response to stromal cell-derived factor 1α (CXCL12) using transwell chambers pre-coated with FN or ICAM-1. In contrast to cell adhesion, migration of

both cells was equally enhanced in response to CXCL12 (Fig. 3D). These results indicate that TCR-independent functions of Jurkat-SMS1/kd cells are normal.

Role of membrane SM in TCR-mediated signal transduction

Lipid raft-associated adapter protein, LAT, is an anchor molecule for TCR signals, via phosphotyrosine-based docking motifs (8). We examined tyrosine phosphorylation of LAT and *ZAP-70* following CD3/TCR stimulation of Jurkat-SM+ and Jurkat-SMS1/kd cells. As shown in Fig. 4, CD3 stimulation induced marked tyrosine phosphorylation of LAT (Fig. 4A) and *ZAP-70* (Fig. 4B) in Jurkat-SM+ cells, while phosphorylation was severely impaired in Jurkat-SMS1/kd cells.

LAT contains multiple tyrosine-based motifs which are phosphorylated by *ZAP-70* or *Syk* and initiates assembly with SH2 domain-containing signaling proteins such as PI3K, PLCγ1 and Grb2, allowing extension of the signaling scaffold (39–42). Immunoblotting analysis revealed that the 72 and 25 kDa proteins were *ZAP-70* and Grb2, respectively. Association of LAT with *ZAP-70* and Grb2 was severely decreased in Jurkat-SMS1/kd cells (Fig. 4C).

Since PKCθ is the major isoform of PKC that locates into the immunological synapse and mediates NF-κB activation after CD3/CD28 stimulation (10, 43), we examined the phosphorylation of PKCθ after CD3 stimulation of Jurkat-SMS1/kd and Jurkat-SM+ cells. Cells were stimulated with the indicated concentration of CD3 mAb for 15 min (Fig. 4D) or stimulated with 1.0 μg ml^{-1} of CD3 mAb for the indicated time (Fig. 4E). After stimulation, cells were lysed, electrophoresed and subjected to immunoblot with antibody to PKCθ and phospho-PKCθ. Stimulation of Jurkat-SM+ cells with CD3 mAb induced phosphorylation of PKCθ, whereas Jurkat-SMS1/kd cells contained no detectable phosphorylated PKCθ (Fig. 4D and E).

Role of membrane SM in translocation of signaling molecules and TCR into lipid rafts

It is well known that TCR engagement induces the translocation of the TCR complex and multiple other signaling molecules such as ZAP-70, Vav, SLP-76, PLCγ1 and PKCθ into lipid rafts (4, 5, 44). Therefore, we investigated whether the distribution of signaling molecules and TCR in rafts are different in Jurkat-SMS1/kd compared with Jurkat-SM+ cells following CD3 cross-linking. Lipid rafts were isolated using equilibrium sucrose density gradients as described (17). The position of the membrane rafts in the sucrose gradient was determined by the presence of *lck* and LAT as well as a well-established raft-associated marker, ganglioside GM1. As shown in Fig. 5(A), *lck*, LAT and ganglioside GM1 were enriched in the upper part of the sucrose gradient (fractions 4 and 5), indicating a separation of the lipid rafts from the Triton X-100-soluble membrane. Although *ZAP-70* and phospho-PKCθ were detected in raft fractions of Jurkat-SMS1/kd and Jurkat-SM+ cells prior to stimulation, a substantial activation-induced shift of *ZAP-70* and PKCθ into raft fractions was observed in Jurkat-SM+ cells. In contrast, translocation of *ZAP-70* and PKCθ was severely impaired in Jurkat-SMS1/kd cells (Fig. 5A). We examined the redistribution of TCR,

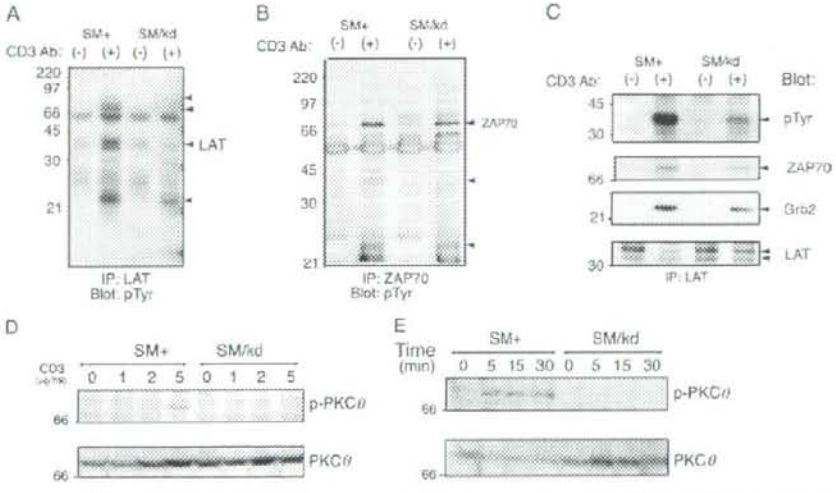

Fig. 4. Role of membrane SM on TCR-mediated signal transduction. Tyrosine phosphorylation of LAT (A) and *ZAP-70* (B). Jurkat-SM+ and Jurkat-SMS1/kd cells were stimulated in the presence or absence of 2 μg ml^{-1} of CD3 mAb for 5 min. LAT and *ZAP-70* were immunoprecipitated and subjected to SDS–PAGE and anti-phosphotyrosine immunoblotting. (C) Association of LAT with *ZAP-70* and Grb2. LAT was immunoprecipitated and subjected to anti-phosphotyrosine (p-Tyr), anti-ZAP-70, anti-Grb2 and anti-LAT immunoblotting. (D) Dose dependency of CD3 mAb on phosphorylation of PKCθ. (E) Time course of PKCθ phosphorylation. Cells were stimulated with the indicated concentration of CD3 mAb for 15 min (D) or stimulated with 5.0 μg ml^{-1} of CD3 mAb for the indicated time (E). After stimulation, cells were lysed and proteins were analyzed by immunoblotting with antibody to PKCθ and phospho-PKCθ (p-PKCθ). These data are representative of more than five independent experiments for (A), (B) and (C) and three independent experiments for (D) and (E), respectively. SM+, Jurkat-SM+ cells; SM/kd, Jurkat-SMS1/kd cells.

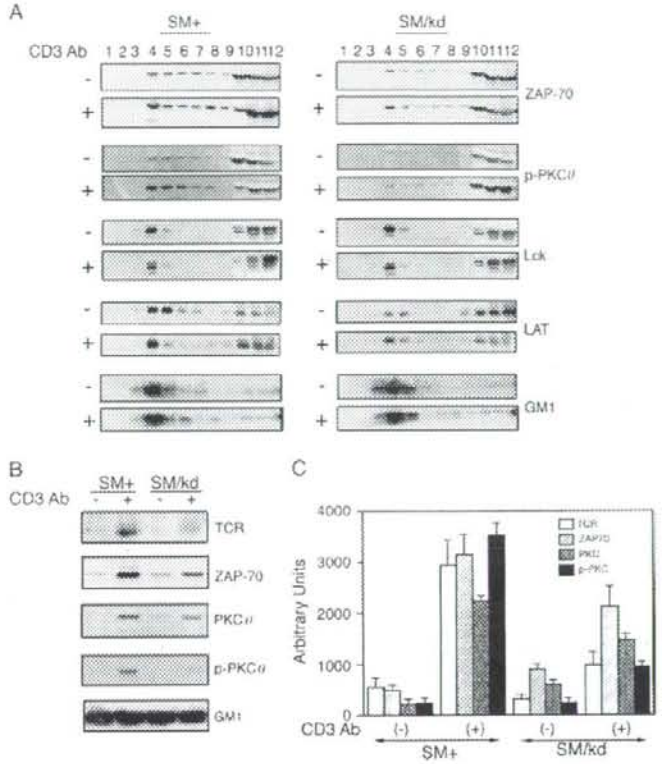

Fig. 5. Role of membrane SM in translocation of signaling molecules into lipid rafts. (A) Lipid rafts fractionation. Cells (2.5×10^8) were left unstimulated (−) or were stimulated with anti-OKT3 mAb for 5 min (+) and Triton X lysates were subjected to sucrose density gradient fractionation. Fractions were run on 15% SDS–PAGE and immunoblotted with antibodies against *ZAP-70*, p-PKCθ and markers for the raft fractions, Lck, LAT and ganglioside GM1. The blots shown are representative of four independent experiments. (B) Redistribution of TCR, *ZAP-70*, PKCθ, p-PKCθ into lipid rafts upon CD3 stimulation. Raft fractions (mixtures of fraction 4 and 5) were run on 15% SDS–PAGE and immunoblotted with the indicated antibodies. (C) Quantification of TCR, *ZAP-70*, PKCθ, p-PKCθ in lipid rafts. Quantification of each band was performed densitometrically using NIH image software and normalized to the amount of ganglioside GM1. Data are average ± SD of three independent experiments and expressed as the arbitrary units.

ZAP-70 and phospho-PKCθ in the raft fractions (fractions 4 and 5) before and after CD3 stimulation several times and compared their translocation in Jurkat-SMS1/kd and Jurkat-SM+ cells (Fig. 5B). As shown in Fig. 5(C), we found that translocation of these signaling molecules is significantly inhibited in Jurkat-SMS1/kd cells compared with Jurkat-SM+ cells after CD3 stimulation.

Discussion

For full T cell activation, the lateral organization of membrane-associated proteins such as the TCR–CD3 complex, PTKs and adaptor molecules are required to sustain the activation signals (8, 11). It has been suggested that sphingolipid- and cholesterol-rich microdomains, lipid rafts, play a key role in protein sorting, signal transduction and cytoskeletal organization to form platforms at the plasma membrane for TCR signaling (1, 3, 5, 6). Raft functions have been analyzed by either disrupting rafts using the cholesterol-chelating reagent, MβCD, or by disrupting the targeting of signaling proteins to rafts. To examine the role of major rafts component, SM, in T cell function, we established the membrane SM-deficient cell line, Jurkat-SMS1/kd, by transfection of *SMS1*-siRNA into Jurkat T cells. *SMS1* gene copy number and SMS activity were decreased in the Jurkat-SMS1/kd cells to ~60% of Jurkat-SM+ cells (Fig. 1A and B). However, reduction in SM levels in Jurkat-SMS1/kd cells was only minor (23%) compared with Jurkat-SM+ cells (Fig. 1C). This discrepancy may be explained by uptake of SM from serum into the medium. An alternative explanation could be that *SMS2* and *SMSr* may substitute SMS levels. Reduction of SMS activity and membrane SM levels in Jurkat-SMS1/kd cells are similar to those in *SMS1*-siRNA-treated cells previously reported (45, 46).

It has been reported that lysenin specifically binds SM only when SM is in the form of a cluster (33). Jurkat-SMS1/kd cells

were negative for lysenin staining (Fig. 1F and G) and resistant to lysenin-mediated lysis (Fig. 1D and E). Although cellular SM levels were not markedly different, we consider the membrane SM level strongly decreased in Jurkat-SMS1/kd cells. Using this system, we found that CD3-induced tyrosine phosphorylation of LAT and threonine phosphorylation of PKCθ were severely inhibited in Jurkat-SMS1/kd cells compared with those in Jurkat-SM+ cells (Fig. 4A, D and E). Moreover, decreased tyrosine phosphorylation of LAT was accompanied by decreased association of *ZAP-70* and Grb2 (Fig. 4C). These inhibitions may result in impaired CD3-mediated cellular activation, such as decreased CD69 expression and cell adhesion to FN in Jurkat-SMS1/kd cells (Fig. 3A–C), suggesting that membrane SM has an important role in T cell activation. In contrast, PMA enhanced CD69 expression equally on both Jurkat-SMS1/kd and Jurkat-SM+ cells (Fig. 3B) and migration of both cells was equally enhanced in response to CXCL12 (Fig. 3D). Therefore, raft-independent functions of Jurkat-SMS1/kd cells were considered to be normal, in spite of the fact that contents of SM metabolites like ceramide, sphingosine and sphingosine 1-phosphate may change and have some effects on cellular functions.

Since lipid raft-resident molecules such as *src* family kinases and the ganglioside GM1 relocalize toward the immunological synapse, it appears that the immunological synapse might be described as a large merger of lipid rafts. However, the initial signals during T cell activation, such as tyrosine phosphorylation, calcium mobilization and phosphoinositide metabolism, occur much earlier than immunological synapse formation (47, 48), and TCR-induced activation of *ZAP-70* by *lck* reaches its maximum even before the typical cSMAC has been formed (47). In addition, TCR-mediated tyrosine kinase signaling occurs primarily at the periphery of the synapse (47, 49), suggesting that spatial-temporal activation may regulate immunological synapse formation (50). Recently, Yokosuka *et al.* (12) have reported that microclusters consisting of CD3ζ, *ZAP-70* and SLP-76 were generated continuously at the periphery of immunological synapses and that TCRs at the contact sites were translocated into the cSMAC, whereas most *ZAP-70* and SLP-76 molecules did not move to the cSMAC. Varma *et al.* (13) also reported that TCR signaling is sustained by stabilized microclusters and is terminated in the cSMAC. Both reports suggested that the cSMAC may function in mediating the microcluster-induced stop signal or TCR degradation. However, these reports do not contradict the existence of rafts or their functions for the following reasons. Estimated raft size in resting cells is between 50 and 200 nm, and there is heterogeneity in the partitioning of the proteins residing in rafts. For example, cholesterol extraction destabilizes the membrane microdomains containing *lck*, but not LAT (51). Recently, Nicolau *et al.* have reported that dynamic partitioning into rafts increases specific interprotein collision rates to maximize the biologically relevant function. Therefore, lipid rafts function as reaction chambers that facilitate nanoscale protein–protein interaction (52). These highly dynamic spatial confinements result in a high probability of raft-targeted molecule species to come into the vicinity with each other but with rapidly exchanging individual molecules. Therefore, many tyrosine phosphorylated proteins become concentrated in the rafts at periphery of immunological synapse upon TCR stimulation. It has been reported that these tyrosine phosphorylated proteins including the TCR–CD3 receptor complex, especially hyper-phosphorylated CD3ζ chains, ZAP-70, PLCγ, Vav and Shc, are detected mainly in rafts by biochemical separation. Consistent with previous reports, we found that translocation of TCR, *ZAP-70* and PKCθ into raft fractions was observed in Jurkat-SM+ cells, but was severely impaired in Jurkat-SMS1/kd cells (Fig. 5), suggesting an important role of membrane SM as a lipid raft constituent enabling translocation of signaling molecules into lipid rafts.

Lipid rafts also stabilize and amplify signals resulting from aggregation of rafts to larger complexes, which are accompanied by further recruitment of important signaling mediators such as LAT and associated molecules and TCR components. In this regard, we have previously reported that membrane SM is crucial for Fas/lipid rafts clustering through local ceramide production that may compartmentalize lipid rafts to ceramide-enriched membrane platforms (17). In addition to this mechanism, functional links between the cytoskeletal machinery and lipid rafts seem important for forming signaling platforms, such as the immunological synapse. Membrane rafts appear to be the place where TCRs become associated with actin cytoskeleton (53–55), since disruption of lipid rafts by MβCD abolished the association of the ζ chain with the actin cytoskeleton. Among intermediate actin-binding proteins, the ezrin–radixin–moesin family of proteins associate with lipid rafts and their binding to actin filaments and membrane proteins is regulated by PKCθ that is recruited to the immunological synapse on stimulation (10, 43). In this study, we clearly demonstrate that translocation of PKCθ was severely decreased in Jurkat-SMS1/kd cells (Fig. 5). This decrease may account for impaired TCR/CD3 clustering in Jurkat-SMS1/kd cells (Fig. 2).

Thus, lipid rafts may not only facilitate distinct protein–protein interactions to build signaling complexes by increasing their local concentration and the probability of contacting and interacting with signaling molecules but also form signaling platforms by cytoskeleton-driven events. Segregation of the plasma membrane into distinct domains is an essential element of immune cell activation and dynamic properties of the membrane depend strongly on the lipid composition (56). Changes in lipid composition are shown to alter the distribution of raft-resident proteins (57). Taken altogether, our data indicate that membrane SM is an important component of lipid rafts and crucial for various raft functions.

Funding

Japanese Ministry of Education and Science and Culture, Uehara Memorial Foundation and Kanazawa Medical University Research Foundation (13557160, 15024236, 15390313, 13877075, 15024236, 15390313); JSPS Grant-in-Aid research funds and Uehara Memorial Foundation to Z.-X.J.

Acknowledgements

Authors dedicate this manuscript to Dr E.T.B. and mourn over her unexpected death.

Abbreviation

cSMAC	central supramolecular activation cluster
CTx	cholera toxin B
FN	fibronectin
fPEG-Chol	fluorescein ester of poly(ethyleneglycol)-derivatized cholesterol ether
FRET	fluorescence resonance energy transfer
GAPDH	glyceraldehyde 3-phosphate dehydrogenase
HSA	human serum albumin
ICAM	inter cellular adhesion molecules
LAT	linker for activation of T cell
MBP	maltose-binding protein
MBS	MS-buffered saline
MβCD	methyl-β-cyclodextrin
PI3K	phosphatidylinositol 3 kinase
PKC	protein kinase C
PLCγ	phospholipase Cγ
PMA	phorbol myristate acetate
PMSF	phenylmethylsulfonyl fluoride
PTK	protein tyrosine kinase
SCR	scrambled sequence
siRNA	short-interfering RNA
SM	sphingomyelin
SMS	sphingomyelin synthase
TLC	thin-layer chromatography

References

1 Simons, K. and Ikonen, E. 1997. Functional rafts in cell membranes. *Nature* 387:569.
2 Cherukuri, A., Dykstra, M. and Pierce, S. K. 2001. Floating the raft hypothesis: lipid rafts play a role in immune cell activation. *Immunity* 14:657.
3 Alonso, M. A. and Millan, J. 2001. The role of lipid rafts in signalling and membrane trafficking in T lymphocytes. *J. Cell. Sci.* 114:3957.
4 Munro, S. 2003. Lipid rafts: elusive or illusive? *Cell* 115:377.
5 Dykstra, M., Cherukuri, A., Sohn, H. W., Tzeng, S.-J. and Pierce, S. K. 2003. Location is everything: lipid rafts and immune cell signaling. *Annu. Rev. Immunol.* 21:457.
6 Viola, A. 2001. The amplification of TCR signaling by dynamic membrane microdomains. *Trends Immunol.* 22:322.
7 Zhang, W., Trible, R. P. and Samelson, L. E. 1998. LAT palmitoylation: its essential role in membrane microdomain targeting and tyrosine phosphorylation during T cell activation. *Immunity* 9:239.
8 Samelson, L. E. 2002. Signal transduction mediated by the T cell antigen receptor: the role of adapter proteins. *Annu. Rev. Immunol.* 20:371.
9 Sun, Z., Arendt, C. W., Ellmeier, W. *et al.* 2000. PKC-θ is required for TCR-induced NF-κB activation in mature but not immature T lymphocytes. *Nature* 404:402.
10 Bi, K., Tanka, Y., Coudronniere, N. *et al.* 2001. Antigen-induced translocation of PKC-theta to membrane rafts is required for T cell activation. *Nat. Immunol.* 2:556.
11 Bromley, S. K., Burack, W. R., Johnson, K. G. *et al.* 2001. The immunological synapse. *Annu. Rev. Immunol.* 19:375.
12 Yokosuka, T., Sakata-Sogawa, K., Kobayashi, W. *et al.* 2005. Newly generated T cell receptor microclusters initiate and sustain T cell activation by recruitment of Zap70 and SLP-76. *Nat. Immunol.* 6:1253.
13 Varma, R., Campi, G., Yokosuka, T., Saito, T. and Dustin, M. L. 2006. T cell receptor-proximal signals are sustained in peripheral microclusters and terminated in the central supramolecular activation cluster. *Immunity* 25:117.
14 Saito, T. and Yokosuka, T. 2006. Immunological synapse and microclusters: the site for recognition and activation of T cells. *Curr. Opin. Immunol.* 18:305.
15 Yamaoka, S., Miyaji, M., Kitano, T., Umehara, H. and Okazaki, T. 2004. Expression cloning of a human cDNA restoring sphingomyelin synthesis and cell growth in sphingomyelin synthase-deficient cells. *J. Biol. Chem.* 279:18688.
16 Huitema, K., van den Dikkenberg, J., Brouwers, J. F. and Holthuis, J. C. 2004. Identification of a family of animal sphingomyelin synthases. *EMBO J.* 23:33.
17 Miyaji, M., Jin, Z. X., Yamaoka, S. *et al.* 2005. Role of membrane sphingomyelin and ceramide in platform formation for Fas-mediated apoptosis. *J. Exp. Med.* 202:249.
18 Jin, Z., Kishi, H., Wei, X., Matsuda, T., Saito, S. and Muraguchi, A. 2002. Lymphoid enhancer-binding factor-1 binds and activates the recombination-activating gene-2 promoter together with c-Myb and Pax-5 in immature B cells. *J. Immunol.* 167:3783.
19 Yamaji-Hasegawa, A., Makino, A., Baba, T. *et al.* 2003. Oligomerization and pore formation of a sphingomyelin-specific toxin, lysenin. *J. Biol. Chem.* 278:22762.
20 Sato, S. B., Ishii, K., Makino, A. *et al.* 2004. Distribution and transport of cholesterol-rich membrane domains monitored by a membrane-impermeant fluorescent polyethylene glycol-derivatized cholesterol. *J. Biol. Chem.* 279:23790.
21 Inoue, H., Yoneda, O., Minami, Y. *et al.* 2002. Lipid rafts as the signaling scaffold for NK cell activation: tyrosine phosphorylation and association of LAT with PI 3-kinase and PLC-γ following CD2 stimulation. *Eur. J. Immunol.* 32:2188.
22 Goda, S., Imai, T., Yoshie, O. *et al.* 2000. CX3C-chemokine, fractalkine enhanced adhesion of THP-1 cells to endothelial cells through integrin-dependent and independent mechanisms. *J. Immunol.* 164:4313.
23 Gouda, S., Inoue, H., Umehara, H. *et al.* 2006. Matrix metalloproteinase-1 produced by human CXCL12-stimulated natural killer cells. *Am. J. Pathol.* 169:445.
24 Goda, S., Quale, A. C., Woods, M. L., Felthauser, A. and Shimizu, Y. 2004. Control of TCR-mediated activation of b1 integrins by the ZAP-70 tyrosine kinase interdomain B region and the linker for activation of T cells adapter protein. *J. Immunol.* 172:5379.
25 Okazaki, T., Bell, R. M. and Hannun, Y. A. 1989. Sphingomyelin turnover induced by vitamin D3 in HL-60 cells. *J. Biol. Chem.* 264:19076.
26 Umehara, H., Huang, J.-Y., Kono, T. *et al.* 1997. Involvement of protein tyrosine kinase p72syk and phosphatidylinositol 3-kinase in CD2-mediated granular exocytosis in natural killer cell line. *J. Immunol.* 159:1200.
27 Takagi, S., Tojo, H., Tomita, S. *et al.* 2003. Alteration of the 4-sphingenine scaffolds of ceramides in keratinocyte-specific Arnt deficient mice affects skin barrier function. *J. Clin. Invest.* 112:1372.
28 Nagatsuka, Y., Tojo, H. and Hirabayashi, Y. 2006. Identification and analysis of novel glycolipids in vertebrate brains by HPLC/mass spectrometry. *Methods Enzymol.* 417:155.
29 Han, X. and Gross, R. 2001. Quantitative analysis and molecular species fingerprinting of triacylglyceride molecular species directly from lipid extracts of biological samples by electrospray ionization tandem mass spectrometry. *Anal. Biochem.* 295:88.
30 Umehara, H., Huang, J.-Y., Kono, T. *et al.* 1998. Co-stimulation of T cells with CD2 augments TCR-CD3-mediated activation of protein tyrosine kinase p72syk, resulting in increased tyrosine phosphorylation of adapter proteins, Shc and Cbl. *Int. Immunol.* 10:833.
31 Taguchi, Y., Kondo, T., Watanabe, M. *et al.* 2004. Interleukin-2-induced survival of natural killer (NK) cells involving phosphatidylinositol-3 kinase-dependent reduction of ceramide through acid sphingomyelinase, sphingomyelin synthase and glucosylceramide synthase. *Blood* 104:3285.
32 Yamaji, A., Sekizawa, Y., Emoto, K. *et al.* 1998. Lysenin, a novel sphingomyelin-specific binding protein. *J. Biol. Chem.* 273:5300.
33 Kobayashi, T., Takahashi, M., Nagatsuka, Y. and Hirabayashi, Y. 2006. Lipid rafts: new tools and a new component. *Biol. Pharm. Bull.* 29:1526.
34 Kiyokawa, E., Baba, T., Otsuka, N., Makino, A., Ohno, S. and Kobayashi, T. 2005. Spatial and functional heterogeneity of sphingolipid-rich membrane domains. *J. Biol. Chem.* 280:24072.
35 Davis, D. M. and Dustin, M. L. 2004. What is the importance of the immunological synapse? *Trends Immunol.* 25:323.
36 Rodgers, W., Farris, D. and Mishra, S. 2005. Merging complexes: properties of membrane raft assemble during lymphocyte signaling. *Trends Immunol.* 26:97.

37 Sancho, D., Gomez, M. and Sanchez-Madrid, F. 2005. CD69 is an immunoregulatory molecule induced following activation. *Trends Immunol.* 26:136.
38 Dustin, M. L., Bivona, T. G. and Philips, M. R. 2004. Membranes as messengers in T cell adhesion signaling. *Nat. Immunol.* 5:363.
39 Tomlinson, M. G., Lin, J. and Weiss, A. 2000. Lymphocytes with a complex: adapter proteins in antigen receptor signaling. *Immunol. Today* 21:584.
40 Rudd, C. E. 1999. Adaptors and molecular scaffolds in immune cell signaling. *Cell* 96:5.
41 van Oers, N. S. C. 1999. T cell receptor-mediated signs and signals governing T cell development. *Semin. Immunol.* 11:227.
42 van Leeuwen, J. E. M. and Samelson, L. E. 1999. T cell antigen-receptor signal transduction. *Curr. Opin. Immunol.* 11:242.
43 Huang, J., Lo, P.-F., Zal, T. *et al.* 2002. CD28 plays a critical role in the segregation of PKCθ within the immunologic synapse. *Proc. Natl Acad. Sci. USA* 99:9369.
44 Harder, T. 2004. Lipid raft domains and protein networks in T-cell receptor signal transduction. *Curr. Opin. Immunol.* 16:353.
45 Li, Z., Hailemariam, T. K., Zhou, H. *et al.* 2007. Inhibition of sphingomyelin synthase (SMS) affects intracellular sphingomyelin accumulation and plasma membrane lipid organization. *Biochim. Biophys. Acta* 1771:1184.
46 Tafesse, F. G., Huitema, K., Hermansson, M. *et al.* 2007. Both sphingomyelin synthases SMS1 and SMS2 are required for sphingomyelin homeostasis and growth in human Hela cells. *J. Biol. Chem.* 282:17537.
47 Lee, K.-H., Holdorf, A. D., Dustin, M. L., Chan, A. C., Allen, P. M. and Shaw, A. S. 2002. T cell receptor signaling precedes immunological synapse formation. *Science* 295:1539.
48 Irvine, D., Purbhoo, M., Krogsgaard, M. and Davis, M. 2002. Direct observation of ligand recognition by T cells. *Nature* 419:845.
49 Freiberg, B. A., Kupfer, H., Maslanik, W. *et al.* 2002. Staging and resetting T cell activation in SMACs. *Nat. Immunol.* 3:911.
50 Mossman, K. D., Campi, G., Groves, J. T. and Dustin, M. L. 2005. Altered TCR signaling from geometrically repatterned immunological synapses. *Science* 310:1191.
51 Schade, A. E. and Levine, A. D. 2002. Lipid raft heterogeneity in human peripheral blood T lymphoblasts: a mechanism for regulating the initiation of TCR signal transduction. *J. Immunol.* 168:2233.
52 Nicolau, D. V. J., Burrage, K., Parton, R. G. and Hancock, J. F. 2006. Identifying optimal lipid raft characteristics required to promote nanoscale protein-protein interactions on the plasma membrane. *Mol. Cell. Biol.* 26:313.
53 Dustin, M. L. and Cooper, J. A. 2000. The immunological synapse and the actin cytoskeleton: molecular hardware for T cell signaling. *Nat. Immunol.* 1:23.
54 Hogg, N., Laschinger, M., Giles, K. and McDowall, A. 2003. T-cell integrins: more than just sticking points. *J. Cell Sci.* 116:4695.
55 Zeyda, M. and Stulnig, T. M. 2006. Lipid rafts & Co.: an integrated model of membrane organization in T cell activation. *Prog. Lipid Res.* 45:187.
56 Harder, T., Rentero, C., Zech, T. and Gaus, K. 2007. Plasma membrane segregation during T cell activation: probing the order of domains. *Curr. Opin. Immunol.* 19:470.
57 Garner, A. E., Smith, D. A. and Hooper, N. M. 2007. Sphingomyelin chain length influences the distribution of GPI-anchored proteins in rafts in supported lipid bilayers. *Mol. Membr. Biol.* 24:233.